Downregulation of astrocytic C3 production alleviates neuronal mitochondrial dysfunction in tauopathy models

Chenxu Lei[1], Bocheng Zhang[1], Risako Tamura[1], Junji Yamaguchi[2 3], Xingyu Cao[1], Yunhui Liu[1], Masahide Seki[4], Yutaka Suzuki[4 5], Kuninori Suzuki[1 6], Isei Tanida[3], Yasuo Uchiyama[3], Tatsuhiro Hisatsune[1*]

[1] Department of Integrated Biosciences, Graduate School of Frontier Sciences, The University of Tokyo, Kashiwa, Chiba, Japan.
[2] Laboratory of Morphology and Image Analysis, Biomedical Research Core Facilities, Juntendo University Graduate School of Medicine, Tokyo, Japan.
[3] Department of Cellular and Molecular Neuropathology, Juntendo University Graduate School of Medicine, Tokyo, Japan.
[4] Department of Computational Biology and Medical Sciences, Graduate School of Frontier Sciences, The University of Tokyo, Kashiwa, Chiba, Japan.
[5] Life Science Data Research Center, Graduate School of Frontier Sciences, The University of Tokyo, Kashiwa, Chiba, Japan.
[6] Collaborative Research Institute for Innovative Microbiology, The University of Tokyo, Bunkyo-ku, Tokyo, Japan.

Correspondence
Tatsuhiro Hisatsune, Department of Integrated Biosciences, Graduate School of Frontier Sciences, The University of Tokyo, Kashiwa, Chiba, Japan. E-mail: Hisatsune@edu.k.u-tokyo.ac.jp

Abstract

Astrocytic complement system over-activation is linked to the progression of neuronal dysfunction and degeneration in neurodegenerative disorders such as Alzheimer's Disease (AD) and tauopathies. Blocking Complement C3 (C3) expression rescues neuronal dysfunction and loss in tauopathy models, however, mechanism of C3 mediating neurodegeneration remains unclear. In this study, we found that activated astrocytes can trigger tau-mediated neuronal mitochondrial swelling and dysfunction through C3 over-production. Increased neuronal mitochondrial dysfunction resulted in the activation of the necroptosis pathway. Our data revealed that downregulation of astrocytic C3 production by anserine, a natural imidazole dipeptide that can target astrocytes had the ability to prevent neuronal mitochondrial dysfunction and necroptosis activation, both in the *in vitro* and *in vivo* tauopathy models. Suppression of astrocyte activation and C3 production also rescued the cognitive function and prolonged the survival rate. Our findings reveal the neurotoxic role of astrocytic C3 in mediating neuronal mitochondrial dysfunction and sequent death through promoting tau pathology and suggest the therapies that can downregulate A1 astrocyte activation and C3 secretion such as anserine have a potential role in alleviating this neurotoxic effect.

Keywords: Alzheimer's disease, Tauopathy, Astrocyte, Mitochondrial dysfunction, Necroptosis, Complement C3, Anserine

Introduction

Alzheimer's disease (AD), the most common form of dementia, is a neurodegenerative disease characterized by progressive neuronal loss and cognitive decline [1]. The formation of neurofibrillary tangles (NFTs) composed of hyperphosphorylated tau in the brain is one of the hallmarks of AD. Tau is a kind of microtubule (MT)-associated protein encoded by the *MAPT* gene, mainly expressed in neuronal axons, and has a primary function of promoting assembly and stability of microtubules [2,3]. In tauopathies like AD, tau would become an abnormal hyperphosphorylated state, which is neurotoxic [4,5] and has been considered to link to dysfunction of neuronal network and neurodegeneration [6]. Clinical studies have reported that tau pathology is more associated with the cognitive decline and the progression of neurodegeneration in AD and other tauopathies compared with Aβ pathology [7-9]. Recently, some molecules that are designed to target pathological tau have received positive results [10,11], indicating that therapies targeted tau pathology and tau-mediated neurodegeneration may be an ideal strategy for AD treatment.

Neuronal mitochondrial dysfunction is associated with neurodegeneration progression in tauopathies like AD [12,13]. Evidence has shown that the aggregation of hyperphosphorylated tau in neurons would bring harmful effects on mitochondria function [14,15]. Neurons with pathological tau over-expression exhibited abnormal mitochondrial morphology, impaired mitochondrial dynamics, impaired oxidative phosphorylation and exacerbate oxidative damage [16,17]. Increased mitochondrial dysfunction would activate the necroptosis pathway by RIPK1/RIPK3/MLKL axis for the over-production of ROS [18-20], which has been reported to account for the death of neurons in AD [21-23].

Astrocytes are the most abundant glial cells in the brain and play an important role in supporting neurons by providing energy and metabolic supply [24]. However, in tauopathies like AD, astrocytes would be activated with increased expression of diseased-associated genes [25,26]. This phenotype is called A1 astrocytes. A1 astrocytes are regulated by the NF-κB pathway, which are neurotoxic and would trigger neurodegeneration by secreting pro-inflammatory factors such as complement C3, a typical factor of A1 astrocytes. Astrocytic C3 over-secretion would exacerbate neuronal degeneration and neuronal death by promoting tau pathology [27-29]. Therefore, therapies against astrocyte activation and C3 secretion is considered to be a potential strategy for tauopathies including AD. However, the specific mechanism of C3 to induce neurodegeneration and neuronal loss is still unclarified.

Here in this study, we used different tauopathy models to research the role of astrocyte activation and C3 over-production in neurodegeneration. We found that astrocytic C3 would trigger tau-mediated mitochondrial dysfunction, which resulted in the activation of the necroptosis pathway. Similar effects of astrocytic C3 were also observed in newborn neurons, which led to the impairment of adult hippocampal neurogenesis (AHN). On the other hand, we found that Anserine (beta-alanyl-3-methyl-L-histidine), a natural imidazole dipeptide existing in muscles in vertebrates with anti-inflammatory activity [30-32], had the ability to target astrocytes and downregulate astrocytic C3 secretion via suppressing Tak1-IKK dependent NF-κB activation to alleviate tau-mediated neuronal mitochondrial dysfunction. Anserine treatment also rescued cognitive function and prolonged the survival rate in tauopathy model mice. Our findings first showed that C3 secretion from activated astrocytes triggered neuronal mitochondrial dysfunction and necroptosis activation, which was mediated by tau pathology and revealed the importance of therapies targeted astrocyte activation in alleviating this pathology.

Results

Downregulation of astrocytic C3 secretion alleviated neuronal mitochondrial dysfunction in an *in vitro* tauopathy model

Firstly, to investigate the role of astrocyte activation on neurodegeneration, we established a novel cell culture model using an immortalized neural stem cell line called MSP-1 cells. MSP-1 cells lack P53 and were allowed to proliferate indefinitely without apoptosis and were allowed to be induced to differentiate into neurons and astrocytes as we previously described [33-36]. We firstly induced MSP-1 cells to differentiate into astrocytes and treated the MSP-1 astrocytes with TNF-α (Fig. 1a). As a result, through RNA-Sequencing (RNA-Seq) analysis, Real-Time Quantitative PCR (RT-qPCR) and immunostaining, TNF-α treatment significantly activated the astrocytes by up-regulating NF-κB signaling pathway (Fig. 1d and g), accompanied by increased expression of pro-inflammatory factors represented by *Ccl2*, *Ccl7* and *Cxcl1* (Fig. 1b and h). At the same time, we found the activation of complement system and increased secretion of complement C3 (C3) (Fig. 1e, h and i). Since *C3* is the most common marker of A1 neurotoxic subtype astrocytes regulated by NF-κB signaling [27,29], these results indicated that MSP-1 astrocytes became neurotoxic phenotype after TNF-α treatment. Next, we tried to suppress the activation of MSP-1 astrocytes by Anserine (beta-alanyl-3-methyl-L-histidine), a natural imidazole dipeptide that can inhibit the astrocyte activation in our previous study [37]. As a result, MSP-1 astrocytes pre-treated with anserine showed decreased NF-κB activation and complement activation, accompanied by reduced expression of pro-inflammatory factors such as *C3* that were observed to be up-regulated in the TNF-α group (Fig.1b-i). Further studies showed that anserine could suppress Tak1 phosphorylation to prevent NF-κB activation by Tak1-Ikk axis (Supplementary Fig. 1). These results suggested the ability of anserine on downregulating A1 astrocyte activation and C3 secretion.

Subsequently, we induced MSP-1 cells to differentiate into neurons and treated the MSP-1 neurons with the culture medium of MSP-1 astrocytes induced by TNF-α to study the effects of A1 astrocyte activation on neurons (Supplementary Fig. 3a). In DIV5, almost all the MSP-1 cells express neuron marker such as Map-2 and PSA-NCAM (Supplementary Fig. 3b-d). As a result, MSP-1 neurons treated with culture media (CM) from TNF-α group (TNF CM) showed decreased mitochondrial membrane potential and increased ROS production (Fig. 2a-d), indicating the abnormal mitochondrial function. Through using MitoBright IM to stain the mitochondria, we found that mitochondria in MSP-1 neurons treated with TNF CM were larger than that in sham group (Supplementary Fig. 2), which suggested the morphological changes together with impaired mitochondrial function. For this, we used the scanning electron microscope (SEM) to observe the structure of mitochondria in TNF CM group. As a result, mitochondria in MSP-1 neurons treated with TNF CM exhibited abnormal swollen structures, which accounted for the mitochondrial dysfunction (Fig. 2e and f). On the other hand, we found that MSP-1 neurons treated with CM from the TNF-α+Anserine group (Anserine CM) showed alleviated mitochondrial dysfunction (Fig. 2a-d) and reduced number of abnormal swollen mitochondria (Fig. 2e and f and Supplementary Fig. 2). Since anserine significantly reduced C3 secretion, then we investigated whether the alleviated neuronal mitochondrial dysfunction was because of the downregulation of C3. We used a C3aR antagonist to block the effects of C3. Interestingly, MSP-1 neurons treated with TNF CM+C3aR antagonist also showed reduced number of swollen mitochondria, which resulted in increased mitochondrial membrane potential and reduced ROS production (Fig. 2a-f and Supplementary Fig. 2). These results indicated the crucial role of C3 to induce mitochondrial dysfunction in MSP-1 neurons.

Since tau pathology, which was positive related to C3 expression in AD and tauopathies, has been reported to trigger neuronal mitochondria dysfunction [15,28], we further studied the change of tau-phosphorylation in MSP-1 neurons. As the result of AT8 staining, we found increased tau-phosphorylation level in MSP-1 neurons treated with TNF CM (Fig. 2g and h). Compared with TNF CM group, Anserine CM group and TNF-C3aRa group showed significantly reduced AT8 intensity (Fig. 2g and h). These findings suggested the C3 induced mitochondrial dysfunction by promoting tau pathology in MSP-1 neurons.

Increased mitochondrial dysfunction would activate the necroptosis pathway, which is reported to be activated in AD patients' brains and is regarded as the main reason for neuronal death in AD [20,21]. By staining with the necroptosis marker, p-MLKL, we observed an increased p-MLKL intensity in MSP-1 neurons treated with TNF CM (Supplementary Fig. 3e and g). On the other hand, TNF-α treatment did not induce p-MLKL intensity in MSP-1 neurons (Supplementary Fig. 3f and h), indicating that neuronal necroptosis was induced by neurotoxic factors secreted by activated MSP-1 astrocytes. Noticeably, MSP-1 neurons treated with Anserine CM or TNF CM+C3aRa showed reduced p-MLKL intensity to the same level as the MSP-1 neurons treated with Necrostatin-1 (Nec-1), a necroptosis inhibitor (Supplementary Fig. 3e and g), which revealed that C3 was the crucial factor in necroptosis activation. To further confirmed this, we treated MSP-1 neurons with C3 and observed the similar results such as decreased mitochondrial membrane potential and necroptosis activation accompanied by increased AT8 intensity in MSP-1 treated with C3 (Supplementary Fig. 4). Taken together, these results suggested the role of astrocytic C3 secretion on tau-mediated neuronal mitochondrial dysfunction and subsequent necroptosis activation. In addition, since MSP-1 neurons can also regarded as newborn neurons for the expression of PSA-NCAM and DCX (Supplementary Fig. 2i), C3 may have similar effect both on mature neurons and newborn neurons.

Downregulation of astrocytic C3 secretion alleviated neuronal mitochondrial dysfunction in TE4 tauopathy model mice

Next, to further evaluate the role of astrocyte activation and C3 secretion in tau-mediated neuronal mitochondrial dysfunction, we used tauopathy model mice. Firstly, we utilized human *APOE4* knock-in *MAPT* (P301S) transgenic mice (TE4). TE4 mice have been reported to show severe tau-mediated neurodegeneration accompanied by complement over-activation at about 9 months of age [6,28,38]. Through RNA-Seq analysis using MACS-isolated astrocytes, we found that the expression of pro-inflammatory factors like *Ccl2*, *Ccl4* and *TNF-α* were up-regulated in astrocytes of TE4 mice accompanied by NF-κB activation compared with control mice (Fig. 3a and b and Supplementary Fig. 5a and b). At the same time, we also found the activation of complement system (Supplementary Fig. 5c-e and Supplementary Fig. 6). Then we focused on the changes of astrocyte reactivity and we found a significantly increased expression of reactive astrocyte markers especially A1-specific markers represented by *C3*, *H2-D1* and *H2-T23* (Fig. 3d-f and Supplementary Fig. 7) in astrocytes of TE4 mice. Increased C3 secretion was also confirmed by ELISA and immunostaining (Fig. 3g-i). Moreover, Mfeg8 that regulated A1 astrocyte activation and C3 secretion was significantly downregulated in astrocytes of TE4 mice [39] (Fig. 3b). Consistent with the in vitro study, we treated TE4 mice with anserine from 7 months of age for 8 weeks and the results showed that astrocytes of anserine-treated TE4 mice, TE4 (A) mice showed reduced expression of pro-inflammatory factors and A1 specific markers represented by *C3* (Fig. 3c-g and Supplementary Fig. 7). Anserine treatment also revered Mfeg8 expression (Fig. 3c). Further analysis of common DEGs that up-regulated in TE4 group and

down-regulated in TE4 (A) group by Go Term and KEGG analysis revealed that anserine treatment significantly inhibited the inflammatory responses and complement activation by NF-κB pathway (Supplementary Fig. 5c-e), and this was confirmed by GESA (Supplementary Fig. 6). From the immunostaining, we confirmed the ability of anserine on blocking C3 expression by NF-κB pathway (Fig. 3h and i and Supplementary Fig. 5a and b). These results indicated the activation of A1 astrocytes with C3 over-production in TE4 model mice and the effect of anserine on preventing this.

Then we studied the tau pathology in TE4 mice after downregulation of astrocytic C3 secretion. Compared with TE4 mice, TE4 (A) mice exhibited attenuated tau pathology both in CA1 and DG area, both in AT8 staining and PT181 staining (Supplementary Fig. 8a-f). Noticeably, the expression of C3 in GFAP positive cells had a strong association with tau pathology in TE4 mice, suggesting the contribution of astrocytic C3 secretion on promoting tau pathology (Supplementary Fig. 8g and h), just like we found in the *in vitro* study.

After that, we studied the effects of astrocytic C3 downregulation on neuronal mitochondrial function in TE4 mice. Similar to the *in vitro* study, by SEM, we observed an increased number of abnormal mitochondria in the hippocampus neurons of TE4 mice (Fig. 4a and b). Abnormal mitochondria also exhibited swollen structures with increased size and length (Supplementary Fig. 9), indicating the mitochondrial dysfunction. Compared with TE4 mice, TE4 (A) mice showed a reduced number of abnormal swollen mitochondria in hippocampus neurons (Fig. 4a and b and Supplementary Fig. 9). Then, through using correlative light and electron microscopy (CLEM), we were able to firstly observed the structure of AT8-positive neurons with aggregated tau fibers (Fig. 4e). For this, we compared the difference of mitochondrial structure in neurons with tau fibers aggregation and neurons with no tau fiber. As a results, hippocampal neurons with tau fibers aggregation showed a higher number of abnormal swollen mitochondria (Fig. 4e-g). Our findings directly showed the contribution of p-Tau on neuronal mitochondrial swelling in tauopathy mice, which was associated with mitochondrial dysfunction.

As a core regulator of neuronal death, we found that increased mitochondrial dysfunction led to neurodegeneration and neuronal death in TE4 mice (Supplementary Fig. 10a and b). Interestingly, we observed necroptosis-like structure neurons in the hippocampus area of TE4 mice. These neurons also contained aggregated tau fibers and showed mitochondrial swelling (Supplementary Fig. 10c), suggesting that the activation of neuronal necroptosis in TE4 mice because of the effects of mitochondrial dysfunction caused by tau pathology. For this, we performed p-MLKL staining to investigate neuronal necroptosis in TE4 mice. We also observed the co-location of p-Tau with necroptosis marker p-MLKL (Supplementary Fig. 10d). These indicated that p-Tau induced neuronal necroptosis in TE4 mice. Compared with control mice, TE4 mice showed increased p-MLKL-positive neuron numbers both in the CA1 and DG areas (Supplementary Fig. 10e). At the same time, anserine treatment significantly alleviated the activation of necroptosis in neurons (Supplementary Fig. 10e), which resulted in increased neuronal density (Supplementary Fig. 11). Moreover, we observed a close association of astrocytic C3 expression with the number of p-MLKL positive neurons in TE4 mice (Supplementary Fig. 10f and g). In general, these results revealed that downregulation of C3 secretion resulted in alleviated neuronal mitochondrial dysfunction and necroptosis activation by attenuating tau pathology.

Suppressed astrocyte activation prolonged the survival rate and improved cognitive function in TE4 mice

P301S tau model mice would exhibit paralysis associated with a hunched posture during tau pathology progression, which results in feeding inability and death [6]. Since anti-inflammatory therapy prolonged the survival rate in P301S mice, we compared the survival rate between TE4 mice and TE4 (A) mice from the beginning of anserine treatment and we observed that TE4 (A) mice hardly developed a hunched posture and could easily live over 10 months of age, while only about 55% TE4 mice could alive over 10 months of age (Fig. 5a-c). On the other hand, the anserine treatment also prevented the weight decline in TE4 mice (Fig. 5d). For the paralysis, TE4 mice also showed physiological deficits like grip strength decline. Compared with TE4 mice, the grip strength of TE4 (A) mice was consistent with control mice (Fig. 5e).

Then we evaluated the cognitive function in TE4 mice after anserine treatment through Y-maze and Radial arm maze (RAM) tests. In Y-maze, TE4 mice showed a significant-decrease in alternation rate compared with control mice. At the same time, TE4 mice take more time to find all the rewards in the RAM test (Fig. 5f-k). These results indicated that neuronal necroptosis led to a decline of cognitive function in TE4 mice. Compared with TE4 mice, TE4 (A) mice showed an increased alternation rate in Y-maze (Fig. 5g), and no difference was found in the total number of entries (Fig. 5h). Similar results were found in the RAM test that TE4 (A) mice showed a shorter time to find all the rewards faster than TE4 mice (Fig. 5i-k). These findings indicated that suppressed A1 astrocyte activation by anserine rescued the cognitive function and kept TE4 mice in a healthy state, which may be associated with attenuated tau pathology because of downregulated C3 production.

Downregulation of astrocyte C3 production alleviated mitochondrial dysfunction n newborn neurons in E4-3Tg model mice

Then we studied the effects of astrocyte activation and C3 production on newborn neurons. During AD progression, neuronal dysfunction and degeneration also in the newborn neurons [40]. Recently, Wang and colleagues reported that the activation of astrocytes may affect the number of immature neurons in the aged human hippocampus and they found some key mediators like NF-κB and STAT3 signaling that may inhibit neurogenesis [41]. Besides, C3 has been reported to affect the survival of newborn neurons [42]. We supposed that astrocytic C3 over-production had the same effects on newborn neurons, just like what we found in MSP-1 neurons.

Since tauopathy mice were mostly used to study the neurodegeneration, and there remained contention about the role of tau pathology in neurogenesis [43], we utilized *APOE4* knock-in/APP/PS1/P301S transgenic (E4-3Tg) model mice in which the number of newborn neurons was significantly decreased at 6 months of age (Supplementary Fig. 12a-c). At the same time, we also found a decline survival rate of newborn neurons in E4-3Tg mice (Supplementary Fig. 12f). These results suggested the loss of newborn neurons during the maturation process.

To clarify the mechanism, we isolated newborn neurons by MACS using Anti-PSA-NCAM microbeads from E4-3Tg mice at 6 months of age and did RNA-Seq analysis (Fig. 6a). As a result, we noticed that genes related to synapse plasticity, axon growth, and neuron maturation were down-regulated in newborn neurons of E4-3Tg mice represented by *Syn, shank2*, *Nrn1, NeuronD6* and *Map1a* (Fig. 6b and c and Supplementary Fig. 13). This indicated the dysfunction of the maturation process. At the same time, we also found the down-regulation of genes related to mitochondria, oxidative phosphorylation and electron transport chain (Fig. 6b and d). Moreover, increased oxidative damage response were observed in newborn neurons of E4-3Tg mice (Figure 6b). These findings revealed that mitochondrial dysfunction was also occurred in the newborn neurons in E4-3Tg mice.

On the other hand, newborn neurons in anserine-treated E4-3Tg mice did not show severe mitochondria dysfunction and increased oxidative damage (Fig. 6b and d). Anserine treatment also protected the synapse plasticity and neuronal maturation in newborn neurons (Fig. 6c and Supplementary Fig. 13), which may relate to the decreased p-Tau expression in DCX-positive cells (Fig. 6e and f). As a result, we found an increased number and survival rate of newborn neurons in E4-3Tg (A) mice (Supplementary Fig. 12). These findings indicated the dysfunction of newborn neurons such as impaired synapse plasticity and mitochondrial dysfunction mediated by tau pathology in E4-3Tg mice and the ability of anserine to alleviate this.

Then we checked the astrocyte activation in E4-3Tg mice after anserine treatment. Consistent with the results in TE4 mice, anserine treatment suppressed the activation of astrocytes and C3 expression by suppressing NF-κB pathway (Fig. 6g and h and Supplementary Fig. 14). Reduced astrocytic C3 expression accounted for the alleviated tau-mediated mitochondrial dysfunction in newborn neurons in E4-3Tg (A) mice.

We also studied whether mitochondrial dysfunction would cause necroptosis activation in newborn neurons. Noticeably, compared with the control group, a significantly increased expression of necroptosis-related genes was found in the E4-3Tg group, represented by *RIPK1, RIPK3 and MLKL* (Supplementary Fig.15a-c). Through immunostaining, we observed the expression of p-MLKL in DCX-positive cells, which can be prevented by Nec-1 (Supplementary Fig. 15d and e). Nec-1 treatment also significantly increased the number of DCX-positive cells and increased the survival rate of newborn neurons (Supplementary Fig. 12). These results revealed the activation of the necroptosis pathway in newborn neurons in E4-3Tg mice. We also found the reduced expression of necroptosis-related genes and reduced number of p-MLKL^{+}/DCX^{+} cells after anserine treatment (Supplementary Fig. 15a-h) and we observed a close association between activated astrocytes and DCX-positive cells number in E4-3Tg mice (Supplementary Fig. 15f), which suggested that the suppression of astrocyte activation was linked to rescued AHN and reduced loss of newborn neurons caused by necroptosis activation. Taken together, our findings showed that astrocyte activation and C3 over-production also related to mitochondrial dysfunction and necroptosis activation in newborn neurons.

Suppressed astrocyte activation prolonged the survival rate and improved cognitive function in E4-3Tg mice

Because of the tau pathology, E4-3Tg mice also a showed reduced survival rate (Fig. 7a). We also investigated whether the anserine treatment had the same effects to prolong the survival rate of E4-3Tg mice just like what we found in TE4 mice. Our data showed that anserine also prevented the death of E4-3Tg mice (Fig. 7a). Besides this, we found improved cognitive function in E4-3Tg (A) mice (Fig. 7b-e) in Y-maze and CFC test. Consistent with TE4 mice, these results suggested that improved AHN levels by downregulating astrocytic C3 production rescued the cognitive function and prolonged the survival rate in E4-3Tg mice.

Blocking the effects of anserine on astrocytes restored astrocytic C3 production and neurodegeneration

To further confirm the effect of astrocytic C3 on tau-mediated neurodegeneration, we knock down (KD) the *Pept2*, a transporter of anserine that only expresses in astrocytes by AAV-shPEPT2-PHP.eB [44] (Fig. 8a-c). We expected anserine can be taken by astrocytes and directly affect astrocytes. Interestingly, compared with TE4 (A) mice injected with AAV-Scramble RNA-PHP.eB (TE4 (A)-

shCon), TE4 (A) mice with AAV-shPEPT2-PHP.eB injection (TE4 (A)-shPEPT2) exhibited an increased astrocyte activation and C3 expression in GFAP positive astrocytes (Fig. 8d-f). These results suggested that *Pept2* KD blocked the effects of anserine on A1 astrocyte activation. As a result, TE4 (A)-shPEPT2 mice showed increased p-Tau expression and number of p-MLKL positive neurons compared with TE4 (A)-shCon mice (Fig. 8g-j). We also investigated the cognitive function between TE4 (A)-shPEPT2 mice and TE4 (A)-shCon mice. Noticeably, TE4 (A)-shPEPT2 showed the same alternation rate as TE4 mice in the Y-maze test, while TE4 (A)-shCon mice also showed improved cognitive function (Fig. 8k). These findings confirmed that astrocytic C3 secretion may be the main reason of tau-mediated neurodegeneration and necroptosis activation in TE4 mice. Anserine, which can target astrocytes by *Pept2*, has the ability to downregulate astrocytic C3 production to prevent the neurotoxic effects of A1 activated astrocytes (Fig. 8l).

Discussion

Recent investigations have shown the crucial role of astrocytes in the progression of neurodegeneration diseases represented by AD [25]. In tauopathies like AD, astrocytes would become neurotoxic with up-regulated expression of A1-specific markers represented by C3 to contribute to neuronal loss by promoting tau pathology [27,28,38,45,46]. In this study, we found that C3 secretion from activated astrocytes would trigger tau pathology-mediated neuronal mitochondrial dysfunction and neuronal necroptosis both in the *in vivo* and *in vitro* tauopathy models, which can be alleviated by anserine treatment through downregulation of astrocytic C3 over-production. Besides, our data showed the positive effects of astrocyte C3 suppression on prolonging the survival rate and improving cognitive function in tauopathy model mice. Collectively, this study first showed the role of astrocytic C3 over-production in modulating neuronal mitochondrial dysfunction and subsequent death in tauopathy. We suggested that therapies that downregulate A1 astrocyte activation and C3 secretion such as anserine have a penitential role in alleviating this neurotoxic effect.

Neuronal mitochondrial dysfunction is one of the hallmarks of the progression of dementia like AD [13]. As highly energetic cells, neurons need healthy mitochondria to maintain the neuronal normal function. Impaired mitochondria show impaired oxidative phosphorylation (OXPHOS), impaired mitochondrial dynamics and increased ROS production [15]. Since brain does not have strong ability of antioxidant [47], increased oxidative damage can cause catastrophic damage to neurons [13]. In this study, by using MSP-1 cell line and tauopathy model mice with P301S mutation, we observed increased number of abnormal mitochondria with increased size and length in neurons, named “swollen structure” caused by exacerbated tau pathology. We also found reduced neuronal mitochondrial membrane potential and increased oxidative response in different tauopathy models. At the same time, attenuated tau pathology by suppression astrocytic C3 rescued the neuronal mitochondrial abnormality and dysfunction. Phosphorylated tau has been reported to induce mitochondrial dysfunction [14]. Neurons with pathological tau over-expression showed mitochondrial elongation, leading to neurodegeneration [17]. In aged mice, increased number of swollen mitochondria and mitochondrial dysfunction was found in hippocampal neurons together with increased p-Tau accumulation [48]. Our findings were consistent with these studies and further confirmed the effects of p-Tau on mitochondrial swelling and dysfunction. Besides, pathological tau may destroy mitochondrial dynamics to affect mitochondrial morphology. p-Tau is reported to interact with Drp1 to block mitochondrial fission [17], which explained the mitochondrial swelling that we observed in neurons of different tauopathy models. Some studies have also shown that impairment of Drp1 mediated mitochondrial fission would lead to dysfunction

of mitophagy, which is important to maintain mitochondrial homeostasis by clearing dysfunctional mitochondria [49-51]. Moreover, enhancing neuronal mitophagy can rescue mitochondrial dysfunction and attenuate tau pathology both in culture neurons and tauopathy model mice [52,53]. Therefore, it is possible that impaired mitochondrial dynamics mediated by tau pathology weakened mitophagy, resulting in accumulation of unrepaired swollen mitochondria and exacerbated mitochondrial dysfunction.

Various studies have provided the evidence of the contribution of activated astrocytes on neuronal oxidative stress and neurodegeneration. Increased astrocyte reactivity is accompanied by dementia progression and plasma GFAP level has been regarded as a useful biomarker for dementia prediction [54]. These suggest that astrocyte activation may play a crucial role in dementia progression. Complement system over-activation is accompanied by astrocyte activation with C3 over-production, linking to tau pathology and neurodegeneration [27,28]. In this study, through *in vivo* and *in vitro* tauopathy models, we found that complement C3 secreted by A1 activated astrocytes could induce neuronal mitochondria dysfunction. C3 may contribute mitochondrial dysfunction by promoting tau pathology because we observed that C3 expression had a close correlation with tau pathology. Importantly, hyperphosphorylated tau is regarded as a main trigger for neuronal necroptosis [20]. Just like what we found in MSP-1 neurons, mitochondrial dysfunction led to ROS over-production, which can activate necroptosis pathway [19]. This finding indicated a possible explanation of the contribution of p-Tau on inducing neuronal necroptosis. As the key factor in tauopathy progression, astrocytic C3 mediated neuronal mitochondrial dysfunction and necroptosis activation through promoting tau phosphorylation by C3-C3aR signaling [55,56], which explained the reduced intensity of AT8 and p-MLKL in MSP-1 neurons treated with C3aR antagonist and the association of C3 expression with p-MLKL-positive neurons number in TE4 mice. To date, this study may be the first report of the effects of astrocytic C3 on triggering neuronal mitochondrial dysfunction and necroptosis activation. Our findings filled the knowledge gap about the specific mechanisms between increased astrocytic C3 secretion and neuronal degeneration in tauopathy.

On the other hand, our findings also showed that astrocytic C3 over-production was related to mitochondrial dysfunction and necroptosis in newborn neurons. The activation of diseased-associated astrocytes has also been reported to be linked to AHN impairment during aging [41]. In AD, the survival and maturation of immature neurons are impaired [40,57]. Previous studies discussed the dysfunction of Neural Stem Cells (NSCs) but ignored the impairment of immature neurons during the maturation process [58]. In this study, our RNA-Seq data showed decreased expression genes related to neuron maturation represented by synapse plasticly, which was also found in the immature neurons of AD patients [59]. This confirmed the dysfunction of the maturation process of newborn neurons in E4-3Tg mice. Not shown in the study, we also observed increased expression of *Ctsd* and *Ctsz* in newborn neurons. Autophagy-lysosome dysfunction is reported in AD neurons [60], we thought this may relate to dysfunction of newborn neurons. Besides, our data showed the mitochondrial dysfunction, increased oxidative damage response and necroptosis activation in newborn neurons of E4-3Tg mice, which can be alleviated by C3 downregulation. These results were consistent with the findings in TE4 mice and MSP-1 neurons. Activation of necroptosis pathway explained the reduced survival rate of newborn neurons and the positive effects of Nec-1 in E4-3Tg mice. To date, this is the first report that newborn neurons would loss through the necroptosis pathway during the maturation process. Although we cannot ignore the effects of Aβ for the APP expression, we observed the expression of p-Tau in DCX-positive cells, which was decreased after anserine treatment for the reduced astrocytic C3 secretion.

Since our previous research showed no change of Aβ pathology in anserine treated APP/PS1 model mice [37], we thought that the dysfunction of newborn neurons we observed in E4-3Tg mice was a main result of tau pathology. Similar to the effect on mature neurons, anserine treatment downregulated astrocytic C3 secretion, leading to attenuated tau pathology and protected mitochondrial function in newborn neurons.

Except for alleviating mitochondrial dysfunction, we found an interesting thing that downregulate astrocytic C3 by anserine prolonged the survival rate both in TE4 and E4-3Tg mice. Reduced lifespan is also one of the characteristics of tau pathology progress due to the decreased muscle strength and paralysis [6]. Research has indicated that p-Tau aggregation in the spinal cord leads to the death of motor neurons, which may account for the decreased muscle strength [61]. Reactive astrocytes have been observed in the spinal cord in tauopathy mice [62], therefore, suppressed astrocytic C3 may also prevent the neurodegeneration in the spinal cord. We thought this further revealed the importance of downregulating C3 over-production in anti-aging because the decline of muscle strength and impaired motor function would not only happen in neurodegenerative diseases but also in the aging process itself.

In this study, we found that anserine could suppress A1 astrocyte activation and C3 secretion through inhibiting Tak1-Ikk-dependent NF-κB signaling to prevent the neurotoxic effects mediated by astrocytic C3. For the anti-inflammatory activity, imidazole dipeptides represented by carnosine and anserine have shown positive effects on AD and other neurodegenerative diseases [30,31]. However, it is still unclear how anserine inhibits astrocyte activation. Anserine can be detected in the brain after intake, indicating anserine can cross the BBB and reach the brain like the hippocampus [63]. Since astrocytes have an important supporting role for neurovascular, it is possible that anserine preferentially affects the astrocytes for they are closer to the neurovascular [64]. Through KD the *Pept2*, an anserine transporter only expressed in astrocytes, we found anserine lost the ability to downregulate astrocytes activation and C3 secretion, which suggested anserine can target astrocytes and revealed the potential role of anserine as a supplement for deregulating astrocyte activation. Moreover, our data showed the ability of anserine to suppress the NF-κB signaling by targeting Tak1 mediated Ikk activation. Tak1 or Ikk activation occurs in many other neurodegeneration diseases, therefore, we believed that anserine may have more application value not only in AD and tauopathies and this need to be clarified in the future study.

In summary, our findings in this study revealed the neurotoxic role of astrocytic C3 in mediating neuronal mitochondrial dysfunction and necroptosis activation and indicated that therapies that downregulate astrocyte activation such as anserine have a neuroprotective role to alleviate this.

Methods

Animals

APPswe/PSEN1dE9 (B6/C3) and P301S tau (B6/C3) transgenic model mice were purchased from Jackson Laboratories (Bar Harbor, Maine, USA). APP/PS1 model mice express the Swedish variation of the phenotype, presenting both a chimeric human APP transgene (Mo/HuApp695swe) and a human PS1 transgene (missing exon 9). P301S tau transgenic model mice expressing human P301S 1N4R tau driven by PrP promoter. Human *APOE4* KI (C57BL/6) model mice were purchased from Riken BRC (Koyadai, Tsukuba, Japan). APOE4 KI mice were crossed to APP/PS1 and P301S tau model mice to generate Tau or APP/PS1/Tau mice in human *APOE4* background, called TE4 and E4-3Tg model mice. Only *APOE4* homozygote mice were used for experiment. *APOE4* KI mice were

used as control. All the mice were sorted by age and genotype, kept under a 12-hour light / dark cycle at ~22 °C, and could get food (solid feed MF; Oriental Yeast Co., Ltd., Tokyo, Japan) and water freely.

All animal procedures and experiments in this study were approved by the ethical committee of the University of Tokyo and were conducted according to the guidelines for animal experimentation required by the University of Tokyo.

Anserine treatment

Anserine used in this experiment was purified from salmon muscles (purity>93%, Tokai Bussan, Tokyo, Japan), which only contains anserine and no carnosine. Anserine-treated mice were maintained on a steady dosage of anserine diluted in autoclaved drinking water, at a concentration of 2.0 g/L (10 mg/mouse per day) for 8 weeks. For TE4 mice, anserine treatment was performed from about 7 months of age to 9 months of age. For E4-3Tg mice, anserine treatment was performed from about 4 months of age to 6 months of age. Behavior tests were performed after the end of treatment.

Y-maze

Y-maze was performed to assess short-term spatial memory of mice, which is suitable to show spontaneous alternation behavior. During the 10-min test, mice were placed on starting arm and allowed to explore the maze freely. The sequence and total number of arms entered were recorded by SMART video tracking system (Panlab, Barcelona, Spain). When mice enter 3 different arms in sequence, it is considered an alternation. The alternation rate was calculated as (the total number of arms entered minus 2 / maximum alternations) × 100. After each test session, the maze was cleaned with 70% ethanol solution.

Radial arm maze

Radial arm maze (RAM) was performed to test spatial reference memory of mice. Mice were given limited food (2g /mouse per day) for at least three days before the test until the end of the test. In order to let the mice adapt the maze, mice were allowed to explore the maze and feeding freely for two days (habituation). There was a 20 mg reward in the end in all of the arms during the habituation. Then following the training trial. The training trial was performed for 5 days and two sessions daily with 1-hour intervals. Mice were placed on the start arm and were allowed to find all the rewards which were only placed in 3 arms. The time that mice find all the 3 rewards were recorded by SMART video tracking system (Panlab, Barcelona, Spain) or until 4 min had cost. After each test session, the maze was cleaned with 70% ethanol solution.

Contextual fear conditioning test

Contextual fear conditioning (CFC) test was performed in P.O.BOX 319 (Med Associates Inc., Albans, UK) for 2 consecutive days. The design of the experiment was described previously [65]. Conditioning test was assessed on the first day. Mice were placed into the box wiped with 70% isopropanol (Context A) for 370 seconds and given a sound (85 db, 5000 Hz, 10s) at 128 seconds, 212 seconds, and 296 seconds with an electric shock (0.75 mA, 1s) in the end. 24 hours after the Conditioning test, Context test was performed. Mice were placed into the same box (Context A) for 512 seconds and freezing time was recorded. The freezing behavior was recorded using Video Freeze Software (Med associate, Inc., St. Albans, UK).

Grip strength test

Grip strength test was conducted to evaluate the physiological function of each mouse. Before the test, the grip strength metre (MK-380M; Muromachi Kikai) was cleaned with 70% ethanol solution. Mice were held by the tail and placed on the grip strength metre and make their two limbs grasped the metal grid. Then the operator gently pulled mice away in a direction horizontal to the grid until the two limbs were detached from the grid, and the peak pull-force was recorded. Each test was performed three sessions with 1 min intervals. The mean value was regarded as the grip strength of each mouse (two limbs). At the same time, the weight of each mouse was recorded to rule out the effect of body weight on grip strength.

Immunohistochemical staining

Mice were perfused with TBS to remove blood and with 4% paraformaldehyde (PFA) to fix the brain tissue. Brain samples were taken and postfixed in 4% PFA for 24 hours, then incubated in 30% sucrose/TBS solution for 48 hours. Tissue-Tek OCT compound (Sakura Finetek, Japan) was used to embedded brain samples. All the brain samples were stored at -80 °C before use. Brain samples were sliced into 50-μm-thick coronal sections with a Cryostat (Microm, Germany) and kept in cryoprotectant solution at -30 °C. For immunofluorescence staining, sections were washed twice with 0.3% TBS-X (Triton) for 10 min and blocked with 3% normal donkey serum (NDS) diluted in 0.3% TBS-X for 60 min at room temperature and then incubated with primary antibodies overnight at 4°C with shaking. The primary antibodies used in this study were anti-GFAP (Mouse, 1:1000, Sigma), anti-C3 (Rat, 1:200, Hycult), anti-DCX (Rabbit, 1:500, Cell Signaling), anti-DCX (Sheep, 1:100, R&D Systems), anti-p-p65 (Rabbit, 1:500, Cell Signaling), anti-p-MLKL (Rabbit, 1:500, Abcam), anti-PT181 (Rat, 1:500, Wako), anti-AT8 (Mouse, 1:500, Thermo Fisher) , anti-NeuN (Mouse, 1:500, Millipore), anti-BrdU (Rat, 1:100, Abcam) and anti-GFP (Rabbit, 1:500, MBL life science). Sections were then washed 3 times with TBS for 10 min and incubated with second antibodies for 2 hours at room temperature. The second antibodies used in this study were donkey anti-mouse IgG Alexa 647 (1:1000, Invitrogen), donkey anti-mouse IgG donkey Alexa 488 (1:1000, Invitrogen), goat anti-rabbit IgG Alexa 488 (1:1000, Invitrogen), donkey anti-rabbit IgG donkey Alexa 568 (1:1000, Invitrogen), goat anti-Rat IgG Alexa 594 (1:1000, Invitrogen) and donkey anti-sheep IgG NL557 (1:200, Jackson Immunoresearch). After wishing with TBS for 10 min, sections were incubated with DAPI (1: 10000, Sigma) in TBS for 5 min and then wished with TBS 2 times for 15 min. For NeuN staining, sections do not need to incubate with DAPI. Sections were finally mounted on microscope slides and visualized using a confocal microscope (FV3000-L4EN-TN21; Olympus, Japan).

Images analysis of immunohistochemical staining

Microscopy images were analyzed with ImageJ software. For stain area analysis like AT8 and PT181 staining, immunoreactivity was quantified by the coverage area of the specific organization. The data was presented as the area % immunoreactivity ± S.E.M. per group. For cell counting analysis like p-MLKL and GFAP staining, the data was presented as the number of positive cells ± S.E.M. per group. For quantification of staining density in specific cells like p-p65 and C3, the staining area was calculated separately using ImageJ and then the staining density of the target factor in the cell was calculated as area %. More than 12 random cells were selected from 4 random acquisition areas for analysis of each mouse. The data was presented as the area in cells ± S.E.M. per group.

For each AT8 or PT181 staining image, AT8 or PT181 positive cells were counted as NFT. Data

was presented as number of NFTs per section ± S.E.M. per group.

For counting the number of DCX-positive and BrdU-positive cells, the entire DG area was analyzed by moving the entire z-axis, and all images were collected. Each image corresponded to a thickness of 1.0 μm. All the images were opened used ImageJ, and then the image of the entire space was presented through the "stack-image to stack" step and "stack-Z project" step. The cell count average of each mouse was converted to the total number of cells in DG based on the standard length of the DG. To evaluate the maturation of newborn neurons, we defined mature DCX cells as DCX positive cells whose dendrites extend to the outside the granular cell layer (GCL). For p-MLKL and DCX co-staining, the data was presented as the number of co-labeling cells per section.

For all immunohistochemical staining, at least three random acquisition areas were considered for each brain section and more than two brain sections from Bregma -1.70 to 2.70 were analyzed for each mouse.

Quantification of neuron density

Three brain sections (bregma −1.4, −1.7, and −2.0 mm) from each mouse were used to quantify the neuron density in CA1 and brain section (bregma -2.0 mm) form each mouse was used to quantify the neuron density in DG to exclude the influence of different positions of hippocampus. NeuN staining was performed to identify mature neurons. The numbers of NeuN positive cells were counted. Neuron density was presented as the number of NeuN positive cells in 1 mm^2 ± S.E.M. per group.

Sample preparation for Scanning Electron Microscopy

For observation of scanning electron microscopy (SEM), mice were perfused with TBS and fixed by 2% paraformaldehyde and 2% glutaraldehyde buffered with 0.1 M phosphate buffer (PB), (pH 7.2) as we previous described. Fixed brains were cut into 0.5-1 mm sections and hippocampus parts were obtained. Sections were then treated with 2% OsO4 in PB for 2h, dehydrated with a graded series of ethanol and embedded in epoxy resin (EPOK812, Okenshoji, Tokyo, Japan). Sections were cut into 90 nm thickness with the ultramicrotome (Leica UC7) and then stained with uranyl acetate and lead citrate. After coating, the sections were observed by electron microscope (Regulus 8240, Hitachi High-Tach Corporation, Tokyo, Japan). For the cell samples, fixed cells were treated with 1% OsO4 in PB for 2h and 0.5% uranyl acetate for 30min. Then the samples were dehydrated with a graded series of ethanol and embedded in epoxy resin, cut into 300 nm thickness with the ultramicrotome and stained for SEM observation as we describe above.

Preparation for in-resin correlative light and electron microscopy

For in-resin correlative light and electron microscopy (CLEM), mice were perfused with TBS and fixed by 4% paraformaldehyde and 0.25% glutaraldehyde buffered with 0.1 M PB. After post-fixation overnight with the same solution, brains were stored in 0.1 M PB at 4°C before use. The brains were then sliced into 50-μm-thick sections by semiauto-matic Leica VT1200 vibrating blade microtome and stored in 0.05% Azide buffered with 0.1 M PB at 4°C. Brain sections were stained with primary antibodies and second antibodies and followed by post-fixation by 2% paraformaldehyde and 2% glutaraldehyde buffered with 0.1 M PB for at least 1h. Then brain sections were treated with 1% OsO4 in PB for 15 min, dehydrated with a graded series of ethanol and embedded in epoxy resin (EPOK812, Okenshoji, Tokyo, Japan). Sections were cut into 300 nm thickness with the ultramicrotome (Leica UC7) and observed by Nikon A1RHD25 confocal laser-scanning microscope to identify the target cells.

589 Finally, the same sections were stained with uranyl acetate and lead citrate and observed by electron
590 microscope (Regulus 8240, Hitachi High-Tach Corporation, Tokyo, Japan).
591
592 **Astrocytes and newborn neurons isolation**
593 Magnetic associated cell sorting (MACS) was used to isolate astrocytes and newborn neurons
594 from mouse brain. Mice were sacrificed under deep anesthesia and brains were removed carefully and
595 washed in cold DPBS to remove the blood. Then cortex and hippocampus parts were taken and
596 dissociated into single cell suspension by using Adult Brain Dissociation Kit (Miltenyi Biotec) based
597 on the manufacturer's protocol. For newborn neurons isolation, only hippocampus part was used. Then
598 the astrocytes or newborn neurons were isolated using Anti-ACSA-2 MicroBead Kit or Anti-PSA-
599 NCAM MicroBead Kit (Miltenyi Biotec). Briefly to say, the single cell suspension was incubated with
600 mouse Fcg receptor block reagent at 4°C for 10 min following by anti-ACSA-2 or anti-PSA-NCAM
601 MicroBead at 4°C for 15 min. Targeted cells were collected by MACS with an MS column (Miltenyi
602 Biotec).
603
604 **Adeno-associated virus preparation**
605 The packaging and purification of AAV-shPEPT2 and AAV-Scramble RNA were performed using
606 TransIT-VirusGEN® Transfection Reagent (Mirus) and AAVpro® Purification Kit (Takara Bio, Japan)
607 based on the manufacturer's protocol. pAAV-U6-shPEPT2-EGFP vector and pAAV-U6-
608 scramble_RNA vector were bought from VectorBulider, pHelper vector was a kind gift from Dr. Haruo
609 Okado (Tokyo Metropolitan Institute of Medical Science), and pUCmini-iCAP-PHP.eB vector was
610 bought from addgene (USA). AAV packaging was conducted in HEK293T cells.
611
612 **Intracerebroventricular injection**
613 Intracerebroventricular injection was performed at about 6.5 months of age. TE4 mice were deep
614 anesthesia with a mixed narcotic solution (0.3 mg/kg medetomidine, 4 mg/kg midazolam, and 5 mg/kg
615 butorphanol tartrate, i.p.). Then mice were received injection of 4ul AAV-PHP.eB-U6-ShPEPT2-EGFP
616 or 4ul AAV-PHP.eB-U6-Scramble_RNA-EGFP at both sides of ventricle using following coordinates:
617 anterior-posterior (AP) = −0.4 mm; medial-lateral (ML) = ±1.0 mm; dorsal-ventral (DV) = −2.0 mm).
618 The injection was performed using an auto-nanoliter injector (Nanoject II, Drummond SCI, USA), and
619 the needle was kept at least 5 min after the injection to prevent the backflow of AAV solution. Each
620 mouse was allowed to recover for 2 weeks and anserine treatment would begin at 7 months of age as
621 described above.
622
623 **Nec-1 treatment**
624 For nec-1 treatment in E4-3Tg mice, nec-1 (Selleck) was dissolved in 5%DMSO, 45%PEG300
625 and 50% ddH_2O solution. Each mouse was received intraperitoneal injection with the dose of
626 6.25mg/Kg as previous described twice a week for 8 weeks [66]. After the last injection, the behavior
627 tests were performed.
628
629 **Mouse striatal precursor-1 (MSP-1) cells culture**
630 MSP-1 cells line was obtained from a neural stem cell line established from ventral telencephalon
631 tissue of p53 KO mice as we previous described [35]. MSP-1 cells were cultured in poly-L-
632 lysine/fibronectin-coated (Sigma) dishes with DMEM/F12 medium (Gibco) containing 10% FBS

(Gibco) and fibroblast growth factor (basic-FGF) (10 ng/ml, Wako). This medium was called MSP-1 proliferation medium. Culture medium was replaced with fresh medium every 2 or 3days.

To obtain differentiated astrocytes, MSP-1 cells were harvested and replaced on new dishes overnight with MSP-1 proliferation medium. The next day, replaced the medium with serum-free DMEM/F12 medium containing N-2 supplement (R&D system), Leukemia Inhibitory Factor (LIF) (10 ng/ml, Wako) and Ciliary Neurotrophic Factor (CNTF) (10 ng/ml, Wako). This medium was called astrocytes-differentiation medium. Culture medium was replaced with fresh medium every 2 or 3 days. On day 5, cells were exposed to Tumor Necrosis Factor-α (TNF-α) (100ng/ml, Wako) for 24 hours. For anserine group, cells were pre-treated with L-Anserine (Toronto Research Chemicals) for 2 hours before exposed to TNF-α.

To obtain differentiated neurons, MSP-1 cells were replaced the medium with serum-free DMEM/F12 medium containing N-2 supplement. This medium was called neurons-differentiation medium. Culture medium was replaced with fresh medium every 2 days. On day 5, cells were treated with cultured supernatant of MSP-1 differentiation-induced astrocytes or mouse C3/C3a protein for 24 hours. Nec-1 and C3aR antagonist (SB290157) were bought from Selleck. Mouse C3/C3a protein was bought from MedChemExpress.

Proteins isolation

For isolation of brain proteins, mice were perfused by TBS and hippocampus parts were taken. Tissues were lysed by RIPA buffer containing 1 mM PMSF (Cell signaling), Protease Inhibitor Cocktail (Wako) and Phosphatase Inhibitor Cocktail (Wako) on ice for 1-2h. For cell samples, harvested cells were lysed by the same RIPA buffer on ice for 30 min. Then, the lysates were centrifuged at 15,000g for 30 min at 4°C and the supernatants were collected (RIPA-soluble fraction). Protein samples were stored at -80 ℃ before use.

Western-Blot

Equal isolated proteins (20-40ug) were electrophoresed by sodium dodecyl sulfate-polyacrylamide gel electrophoresis (SDS-PAGE) and transferred proteins from gel onto polyvinylidene difluoride fluoride (PVDF) membranes (BioRad). After transformation, the blotting membranes were blocked with EveryBlot blocking buffer (BioRad) with shaking for 5 minutes at room temperature. Subsequently, blocked membranes were incubated with diluted primary antibodies at 4 °C overnight. The primary antibodies used in this study were anti-α-Tubulin (Mouse, 1:2000, Proteintech), anti-Tak1 (Rabbit, 1:500, Cell signaling), anti-p-Tak1 (Rabbit, 1:500, Cell signaling), anti-IKK (Rabbit, 1:1000, Proteintech), anti-p-IKK (Rabbit, 1:500, Cell signaling) and anti-p-IκB (Rabbit, 1:1000, Cell signaling). All the membranes would be washed with 0.05% TBS-T for five cycles for five minutes each, the membranes were then incubated with diluted secondary antibodies for one hour at 37 ℃. The secondary antibodies used in this study were HRP-conjugated Goat Anti-Mouse IgG (1:10000, Proteintech) and HRP-conjugated Goat Anti-Rabbit IgG (1:10000, Proteintech). Following, the membranes processed the same washing procedure as before. Finally, Clarity Max Western ECL Substrate (BioRad) and Image Gauge version 3.41 (Fuji Film, Japan) was used to detect the signals. Relative expression of target protein was analyzed by Image J using α-Tubulin as a host protein.

Immunocytochemistry staining

Harvested MSP-1 cells were cultured in poly-L-lysine/fibronectin-coated chamber glass (4 wells or 8 wells, Watson) with MSP-1 differentiation medium to get astrocytes or neurons differentiation. After treatment, cells were fixed with 4% PFA for 10 min and following a wash in TBS for 10 min. Then cells were blocked with 5% BSA diluted in 0.05% TBS-T for 30 min at room temperature and then incubated with blocking solution contained primary antibodies overnight at 4°C. The primary antibodies used in this study were anti-AT8 (mouse, 1:1000, Thermo fisher), anti-PSA-NCAM (mouse, 1:1000, gift from Dr. Seki), anti-DCX (mouse, 1:1000, Santa Cruz), anti-MAP2 (Rabbit, 1:1000, Proteintech), anti-p-p65 (rabbit, 1:500, Cell signaling), anti-p-Ikk (Rabbit, 1:1000, Cell signaling), anti-p-Tak1 (rabbit, 1:1000, Cusabio) and anti-p-MLKL (Rabbit, 1:2000, Abcam). Cells were then washed 3 times with TBS for 5 min and incubated with second antibodies for 2 hours at room temperature. The second antibodies used in this study were donkey anti-mouse IgG Alexa 488 (1:1000, Molecular Probes), goat anti-mouse IgM Alexa 488 (1:1000, Abcam) and donkey anti-rabbit IgG Alexa 568 (1:1000, Molecular Probes). After wishing with TBS for 5 min, sections were incubated with DAPI (1: 10000, Sigma) in TBS for 5 min and then wished with TBS 2 times for 5 min. Cells were visualized using a confocal microscope (FV3000-L4EN-TN21; Olympus, Japan).

Image analysis of immunocytochemistry staining

Microscopy images were analyzed with ImageJ software. For AT8, p-MLKL, p-Tak1 and p-IKK staining, the stain intensity was calculated. The data was presented as the relative intensity (radio to sham) ± S.E.M. per group. For p-p65 staining, only the stain intensity in nucleus was calculated and the data was presented as the relative intensity ± S.E.M. per group. More than 100 cells were analyzed in each group from at least 10 random images.

Mitochondrial function assay

Mitochondrial membrane potential, mitochondrial morphology and oxidative stress in MSP-1 neurons were analyzed using MT-1 MitoMP Detection Kit (Dojindo), Mitobright IM Red (Dojindo) and ROS Assay Kit -Photo-oxidation Resistant DCFH-DA- (Dojindo) according to the manual. Briefly to say, after the CM treatment, cells were treated with corresponding reagents for 30 min and then washed with HBSS. After fixed with 4% paraformaldehyde, Cells were visualized using a confocal microscope (FV3000-L4EN-TN21; Olympus, Japan). Obtained imaged were analyzed by Image J.

RNA sequencing

Total RNA from isolated astrocytes or newborn neurons and MSP-1 differentiation induced astrocytes was isolated using RNeasy Mini Kit (Qiagen).1ng (isolated astrocytes and newborn neurons) or 10ng (cultured astrocytes) RNA samples were pre-treated with SMART-seq stranded Kit (Takara Bio, Japan). The sequencing was performed using Illumina NovaSeq6000 (Illumina, USA).

Transcripts per million (TPM) data was used to evaluate the genes expression levels and different expressed genes (DEGs) were identified by DESeq2 package in R environment. DEGs were further used for Gene Ontology (GO) analysis and Kyoto Encyclopedia of Genes and Genomes (KEGG) pathway analysis using David analysis (https://david.ncifcrf.gov/). Gene set enrichment analysis (GSEA) was performed based on the TPM data using GESA software (UC San Diego and Broad Institute). The figures were generated by ggplot2 package in R environment.

721 **Real-time quantitative PCR (RT-qPCR)**

722 Isolated newborn neurons and astrocytes RNA samples (1-2ng) or cultured MSP-1 astrocytes
723 samples (500ng) were used for Reverse transcription reaction for cDNA synthesis using SuperScript™
724 III Reverse Transcriptase (Thermo Fisher) according to the instruction manuals. RT-qPCR was
725 conducted using TP-850 (Takara Bio, Japan) and TB green Taq (Takara Bio, Japan) with following
726 protocol: an initial 30s denaturation at 95°C, then 5s at 95°C and 30s at 60°C for 50 cycles because of
727 the low concentration of the samples. All the samples were run into double and β-actin was used as a
728 reference gene. Analysis was performed with the $2^{-\Delta\Delta Ct}$ method and expressed as fold changes. The
729 gene sequences for RT-qPCR were designed Primer 3 (Supplementary Table).
730

731 **Statistical analyses**

732 All Data were expressed as the mean ± SEM and were analyzed with GraphPad Prism (version
733 8; GraphPad Software). A two-tailed Student's t-test was used for the statistical comparison of two
734 samples. For groups more than 3, a one-way ANOVA with Tukey post-hoc test was used. For data
735 across days, data were analyzed by two-way ANOVA with a Holm-Sidak post-hoc test was used for
736 Multiple comparison test. A p value less than 0.05 was considered statistically significant.

References

1 Querfurth, H. W. & LaFerla, F. M. Alzheimer's disease. *N Engl J Med* **362**, 329-344 (2010). https://doi.org/10.1056/NEJMra0909142

2 Alonso, A. C., Li, B., Grundke-Iqbal, I. & Iqbal, K. Mechanism of tau-induced neurodegeneration in Alzheimer disease and related tauopathies. *Curr Alzheimer Res* **5**, 375-384 (2008). https://doi.org/10.2174/156720508785132307

3 Mandelkow, E. M. *et al.* Tau domains, phosphorylation, and interactions with microtubules. *Neurobiol Aging* **16**, 355-362; discussion 362-353 (1995). https://doi.org/10.1016/0197-4580(95)00025-a

4 Kovacech, B. & Novak, M. Tau truncation is a productive posttranslational modification of neurofibrillary degeneration in Alzheimer's disease. *Curr Alzheimer Res* **7**, 708-716 (2010). https://doi.org/10.2174/156720510793611556

5 Despres, C. *et al.* Identification of the Tau phosphorylation pattern that drives its aggregation. *Proc Natl Acad Sci U S A* **114**, 9080-9085 (2017). https://doi.org/10.1073/pnas.1708448114

6 Yoshiyama, Y. *et al.* Synapse loss and microglial activation precede tangles in a P301S tauopathy mouse model. *Neuron* **53**, 337-351 (2007). https://doi.org/10.1016/j.neuron.2007.01.010

7 Arriagada, P. V., Growdon, J. H., Hedley-Whyte, E. T. & Hyman, B. T. Neurofibrillary tangles but not senile plaques parallel duration and severity of Alzheimer's disease. *Neurology* **42**, 631-639 (1992). https://doi.org/10.1212/wnl.42.3.631

8 Josephs, K. A. *et al.* Beta-amyloid burden is not associated with rates of brain atrophy. *Ann Neurol* **63**, 204-212 (2008). https://doi.org/10.1002/ana.21223

9 Bejanin, A. *et al.* Tau pathology and neurodegeneration contribute to cognitive impairment in Alzheimer's disease. *Brain* **140**, 3286-3300 (2017). https://doi.org/10.1093/brain/awx243

10 Miller, L. V. *et al.* Co-opting templated aggregation to degrade pathogenic tau assemblies and improve motor function. *Cell* (2024).

11 Benn, J. *et al.* Aggregate-selective removal of pathological tau by clustering-activated degraders. *Science* **385**, 1009-1016 (2024). https://doi.org/10.1126/science.adp5186

12 Song, T. *et al.* Mitochondrial dysfunction, oxidative stress, neuroinflammation, and metabolic alterations in the progression of Alzheimer's disease: A meta-analysis of in vivo magnetic resonance spectroscopy studies. *Ageing Res Rev* **72**, 101503 (2021). https://doi.org/10.1016/j.arr.2021.101503

13 Wang, W., Zhao, F., Ma, X., Perry, G. & Zhu, X. Mitochondria dysfunction in the pathogenesis of Alzheimer's disease: recent advances. *Mol Neurodegener* **15**, 30 (2020). https://doi.org/10.1186/s13024-020-00376-6

14 Pérez, M. J., Jara, C. & Quintanilla, R. A. Contribution of Tau Pathology to Mitochondrial Impairment in Neurodegeneration. *Front Neurosci* **12**, 441 (2018). https://doi.org/10.3389/fnins.2018.00441

15 Guha, S., Johnson, G. V. W. & Nehrke, K. The Crosstalk Between Pathological Tau Phosphorylation and Mitochondrial Dysfunction as a Key to Understanding and Treating Alzheimer's Disease. *Mol Neurobiol* **57**, 5103-5120 (2020). https://doi.org/10.1007/s12035-020-02084-0

16 David, D. C. *et al.* Proteomic and functional analyses reveal a mitochondrial dysfunction in P301L tau transgenic mice. *J Biol Chem* **280**, 23802-23814 (2005). https://doi.org/10.1074/jbc.M500356200

17 DuBoff, B., Götz, J. & Feany, M. B. Tau promotes neurodegeneration via DRP1 mislocalization in vivo. *Neuron* **75**, 618-632 (2012). https://doi.org/10.1016/j.neuron.2012.06.026

18 Baines, C. P. Role of the mitochondrion in programmed necrosis. *Front Physiol* **1**, 156 (2010).

https://doi.org/10.3389/fphys.2010.00156

19 Deragon, M. A. *et al.* Mitochondrial ROS prime the hyperglycemic shift from apoptosis to necroptosis. *Cell Death Discov* **6**, 132 (2020). https://doi.org/10.1038/s41420-020-00370-3

20 Dong, Y. *et al.* Hyperphosphorylated tau mediates neuronal death by inducing necroptosis and inflammation in Alzheimer's disease. *J Neuroinflammation* **19**, 205 (2022). https://doi.org/10.1186/s12974-022-02567-y

21 Caccamo, A. *et al.* Necroptosis activation in Alzheimer's disease. *Nat Neurosci* **20**, 1236-1246 (2017). https://doi.org/10.1038/nn.4608

22 Jayaraman, A., Htike, T. T., James, R., Picon, C. & Reynolds, R. TNF-mediated neuroinflammation is linked to neuronal necroptosis in Alzheimer's disease hippocampus. *Acta Neuropathol Commun* **9**, 159 (2021). https://doi.org/10.1186/s40478-021-01264-w

23 Koper, M. J. *et al.* Necrosome complex detected in granulovacuolar degeneration is associated with neuronal loss in Alzheimer's disease. *Acta Neuropathol* **139**, 463-484 (2020). https://doi.org/10.1007/s00401-019-02103-y

24 Liddelow, S. A. & Barres, B. A. Reactive Astrocytes: Production, Function, and Therapeutic Potential. *Immunity* **46**, 957-967 (2017). https://doi.org/10.1016/j.immuni.2017.06.006

25 Rodríguez-Arellano, J. J., Parpura, V., Zorec, R. & Verkhratsky, A. Astrocytes in physiological aging and Alzheimer's disease. *Neuroscience* **323**, 170-182 (2016). https://doi.org/10.1016/j.neuroscience.2015.01.007

26 González-Reyes, R. E., Nava-Mesa, M. O., Vargas-Sánchez, K., Ariza-Salamanca, D. & Mora-Muñoz, L. Involvement of Astrocytes in Alzheimer's Disease from a Neuroinflammatory and Oxidative Stress Perspective. *Front Mol Neurosci* **10**, 427 (2017). https://doi.org/10.3389/fnmol.2017.00427

27 Liddelow, S. A. *et al.* Neurotoxic reactive astrocytes are induced by activated microglia. *Nature* **541**, 481-487 (2017). https://doi.org/10.1038/nature21029

28 Wu, T. *et al.* Complement C3 Is Activated in Human AD Brain and Is Required for Neurodegeneration in Mouse Models of Amyloidosis and Tauopathy. *Cell Rep* **28**, 2111-2123.e2116 (2019). https://doi.org/10.1016/j.celrep.2019.07.060

29 Lian, H. *et al.* NFκB-activated astroglial release of complement C3 compromises neuronal morphology and function associated with Alzheimer's disease. *Neuron* **85**, 101-115 (2015). https://doi.org/10.1016/j.neuron.2014.11.018

30 Masuoka, N., Lei, C., Li, H. & Hisatsune, T. Influence of Imidazole-Dipeptides on Cognitive Status and Preservation in Elders: A Narrative Review. *Nutrients* **13** (2021). https://doi.org/10.3390/nu13020397

31 Masuoka, N. *et al.* Anserine, HClO-scavenger, protected against cognitive decline in individuals with mild cognitive impairment. *Aging (Albany NY)* **13** (2021). https://doi.org/10.18632/aging.202535

32 Boldyrev, A. A., Aldini, G. & Derave, W. Physiology and pathophysiology of carnosine. *Physiol Rev* **93**, 1803-1845 (2013). https://doi.org/10.1152/physrev.00039.2012

33 Kaji, T., Kaieda, I., Hisatsune, T. & Kaminogawa, S. 3-Morpholinosydnonimine hydrochloride induces p53-dependent apoptosis in murine primary neural cells: a critical role for p21(ras)-MAPK-p19(ARF) pathway. *Nitric Oxide* **6**, 125-134 (2002). https://doi.org/10.1006/niox.2001.0389

34 Hisatsune, T., Yamada, K., McKay, R. & Kaminogawa, S. in *Animal Cell Technology: Basic & Applied Aspects: Proceedings of the Ninth Annual Meeting of the Japanese Association for Animal*

Cell Technology, Yokohama, Japan, September 1–4, 1996. 17-22 (Springer).

35 Kaji, T., Yoshida, N., Yamada, K., Hisatsune, T. & Kaminogawa, S. Establishment and characterization of immortalized hippocampal neural precursor cell lines. *Cytotechnology* **33**, 53-61 (2000). https://doi.org/10.1023/a:1008159211932

36 Muramatsu, D., Sato, Y., Hishiyama, S., Miyamoto, Y. & Hisatsune, T. Transplantation of GABAergic neurons into adult mouse neocortex. *Exp Neurol* **194**, 1-11 (2005). https://doi.org/10.1016/j.expneurol.2005.01.025

37 Kaneko, J., Enya, A., Enomoto, K., Ding, Q. & Hisatsune, T. Anserine (beta-alanyl-3-methyl-L-histidine) improves neurovascular-unit dysfunction and spatial memory in aged AβPPswe/PSEN1dE9 Alzheimer's-model mice. *Sci Rep* **7**, 12571 (2017). https://doi.org/10.1038/s41598-017-12785-7

38 Shi, Y. *et al.* ApoE4 markedly exacerbates tau-mediated neurodegeneration in a mouse model of tauopathy. *Nature* **549**, 523-527 (2017). https://doi.org/10.1038/nature24016

39 Xu, X. *et al.* MFG-E8 reverses microglial-induced neurotoxic astrocyte (A1) via NF-κB and PI3K-Akt pathways. *J Cell Physiol* **234**, 904-914 (2018). https://doi.org/10.1002/jcp.26918

40 Moreno-Jiménez, E. P. *et al.* Adult hippocampal neurogenesis is abundant in neurologically healthy subjects and drops sharply in patients with Alzheimer's disease. *Nat Med* **25**, 554-560 (2019). https://doi.org/10.1038/s41591-019-0375-9

41 Wang, W. *et al.* Transcriptome dynamics of hippocampal neurogenesis in macaques across the lifespan and aged humans. *Cell Res* **32**, 729-743 (2022). https://doi.org/10.1038/s41422-022-00678-y

42 Westacott, L. J. *et al.* Dissociable effects of complement C3 and C3aR on survival and morphology of adult born hippocampal neurons, pattern separation, and cognitive flexibility in male mice. *Brain Behav Immun* **98**, 136-150 (2021). https://doi.org/10.1016/j.bbi.2021.08.215

43 Houben, S. *et al.* Tau Pathology and Adult Hippocampal Neurogenesis: What Tau Mouse Models Tell us? *Front Neurol* **12**, 610330 (2021). https://doi.org/10.3389/fneur.2021.610330

44 Xiang, J., Hu, Y., Smith, D. E. & Keep, R. F. PEPT2-mediated transport of 5-aminolevulinic acid and carnosine in astrocytes. *Brain Res* **1122**, 18-23 (2006). https://doi.org/10.1016/j.brainres.2006.09.013

45 Linnerbauer, M., Wheeler, M. A. & Quintana, F. J. Astrocyte Crosstalk in CNS Inflammation. *Neuron* **108**, 608-622 (2020). https://doi.org/10.1016/j.neuron.2020.08.012

46 Litvinchuk, A. *et al.* Complement C3aR Inactivation Attenuates Tau Pathology and Reverses an Immune Network Deregulated in Tauopathy Models and Alzheimer's Disease. *Neuron* **100**, 1337-1353.e1335 (2018). https://doi.org/10.1016/j.neuron.2018.10.031

47 Cassidy, L. *et al.* Oxidative stress in alzheimer's disease: A review on emergent natural polyphenolic therapeutics. *Complement Ther Med* **49**, 102294 (2020). https://doi.org/10.1016/j.ctim.2019.102294

48 Torres, A. K., Jara, C., Olesen, M. A. & Tapia-Rojas, C. Pathologically phosphorylated tau at S396/404 (PHF-1) is accumulated inside of hippocampal synaptic mitochondria of aged Wild-type mice. *Sci Rep* **11**, 4448 (2021). https://doi.org/10.1038/s41598-021-83910-w

49 Kerr, J. S. *et al.* Mitophagy and Alzheimer's Disease: Cellular and Molecular Mechanisms. *Trends Neurosci* **40**, 151-166 (2017). https://doi.org/10.1016/j.tins.2017.01.002

50 Twig, G. *et al.* Fission and selective fusion govern mitochondrial segregation and elimination by autophagy. *Embo j* **27**, 433-446 (2008). https://doi.org/10.1038/sj.emboj.7601963

51 Lin, X. H. *et al.* Suppressing DRP1-mediated mitochondrial fission and mitophagy increases mitochondrial apoptosis of hepatocellular carcinoma cells in the setting of hypoxia. *Oncogenesis* **9**, 67 (2020). https://doi.org/10.1038/s41389-020-00251-5

52 Fang, E. F. *et al.* Mitophagy inhibits amyloid-β and tau pathology and reverses cognitive deficits in models of Alzheimer's disease. *Nat Neurosci* **22**, 401-412 (2019). https://doi.org/10.1038/s41593-018-0332-9

53 Kshirsagar, S., Sawant, N., Morton, H., Reddy, A. P. & Reddy, P. H. Mitophagy enhancers against phosphorylated Tau-induced mitochondrial and synaptic toxicities in Alzheimer disease. *Pharmacol Res* **174**, 105973 (2021). https://doi.org/10.1016/j.phrs.2021.105973

54 Guo, Y. *et al.* Plasma proteomic profiles predict future dementia in healthy adults. *Nat Aging* (2024). https://doi.org/10.1038/s43587-023-00565-0

55 Yao, Y. *et al.* Complement C3a receptor antagonist alleviates tau pathology and ameliorates cognitive deficits in P301S mice. *Brain Res Bull* **200**, 110685 (2023). https://doi.org/10.1016/j.brainresbull.2023.110685

56 Hu, J. *et al.* Complement C3a receptor antagonist attenuates tau hyperphosphorylation via glycogen synthase kinase 3β signaling pathways. *Eur J Pharmacol* **850**, 135-140 (2019). https://doi.org/10.1016/j.ejphar.2019.02.020

57 Tobin, M. K. *et al.* Human Hippocampal Neurogenesis Persists in Aged Adults and Alzheimer's Disease Patients. *Cell Stem Cell* **24**, 974-982.e973 (2019). https://doi.org/10.1016/j.stem.2019.05.003

58 Disouky, A. & Lazarov, O. Adult hippocampal neurogenesis in Alzheimer's disease. *Prog Mol Biol Transl Sci* **177**, 137-156 (2021). https://doi.org/10.1016/bs.pmbts.2020.09.002

59 Zhou, Y. *et al.* Molecular landscapes of human hippocampal immature neurons across lifespan. *Nature* **607**, 527-533 (2022). https://doi.org/10.1038/s41586-022-04912-w

60 Nixon, R. A. & Rubinsztein, D. C. Mechanisms of autophagy-lysosome dysfunction in neurodegenerative diseases. *Nat Rev Mol Cell Biol* **25**, 926-946 (2024). https://doi.org/10.1038/s41580-024-00757-5

61 Allen, B. *et al.* Abundant tau filaments and nonapoptotic neurodegeneration in transgenic mice expressing human P301S tau protein. *J Neurosci* **22**, 9340-9351 (2002). https://doi.org/10.1523/jneurosci.22-21-09340.2002

62 López-González, I. *et al.* Neuroinflammatory Gene Regulation, Mitochondrial Function, Oxidative Stress, and Brain Lipid Modifications With Disease Progression in Tau P301S Transgenic Mice as a Model of Frontotemporal Lobar Degeneration-Tau. *J Neuropathol Exp Neurol* **74**, 975-999 (2015). https://doi.org/10.1097/nen.0000000000000241

63 Tomonaga, S. *et al.* Oral administration of chicken breast extract increases brain carnosine and anserine concentrations in rats. *Nutr Neurosci* **10**, 181-186 (2007). https://doi.org/10.1080/10284150701587338

64 Liu, C. Y., Yang, Y., Ju, W. N., Wang, X. & Zhang, H. L. Emerging Roles of Astrocytes in Neuro-Vascular Unit and the Tripartite Synapse With Emphasis on Reactive Gliosis in the Context of Alzheimer's Disease. *Front Cell Neurosci* **12**, 193 (2018). https://doi.org/10.3389/fncel.2018.00193

65 Herculano, B. *et al.* β-alanyl-L-histidine rescues cognitive deficits caused by feeding a high fat diet in a transgenic mouse model of Alzheimer's disease. *J Alzheimers Dis* **33**, 983-997 (2013). https://doi.org/10.3233/jad-2012-121324

66 Yang, S. H. *et al.* Nec-1 alleviates cognitive impairment with reduction of Aβ and tau abnormalities

in APP/PS1 mice. *EMBO Mol Med* **9**, 61-77 (2017). https://doi.org/10.15252/emmm.201606566

Acknowledgements
We thanked Tokai Bussan for the anserine sample. We thanked Mrs. Izumi Shiraishi and Mrs. Keiko Murasakino for the daily support in the lab. We thanked the gift of pHelper vector from Dr. Haruo Okado. We thanked Dr. Tatsunori Seki for the kindly gift of PSA-NCAM antibody. In additional, this work was supported by JST SPRING, Grant Number JPMJSP2108. Some of the diagrams were created with BioRender.com.

Author Contributions
C.L., I.T., Y.U, K.S. and T.H. designed the experiments. C.L., B.Z., J.Y., R.T., Y.S. and M.S. performed the experiment and collected the data. Y.L., X.C., J.Y., I.T., Y.U and K.S. prepared the reagents, materials and instruments. C.L. and B.Z. analyzed the data and prepared the figures. C.L., B.Z., I.T., Y.U and T.H prepared the manuscript with the assistance of other authors. All authors have read this manuscript and approved the manuscript.

Competing interests:
Authors declare that they have no competing interests.

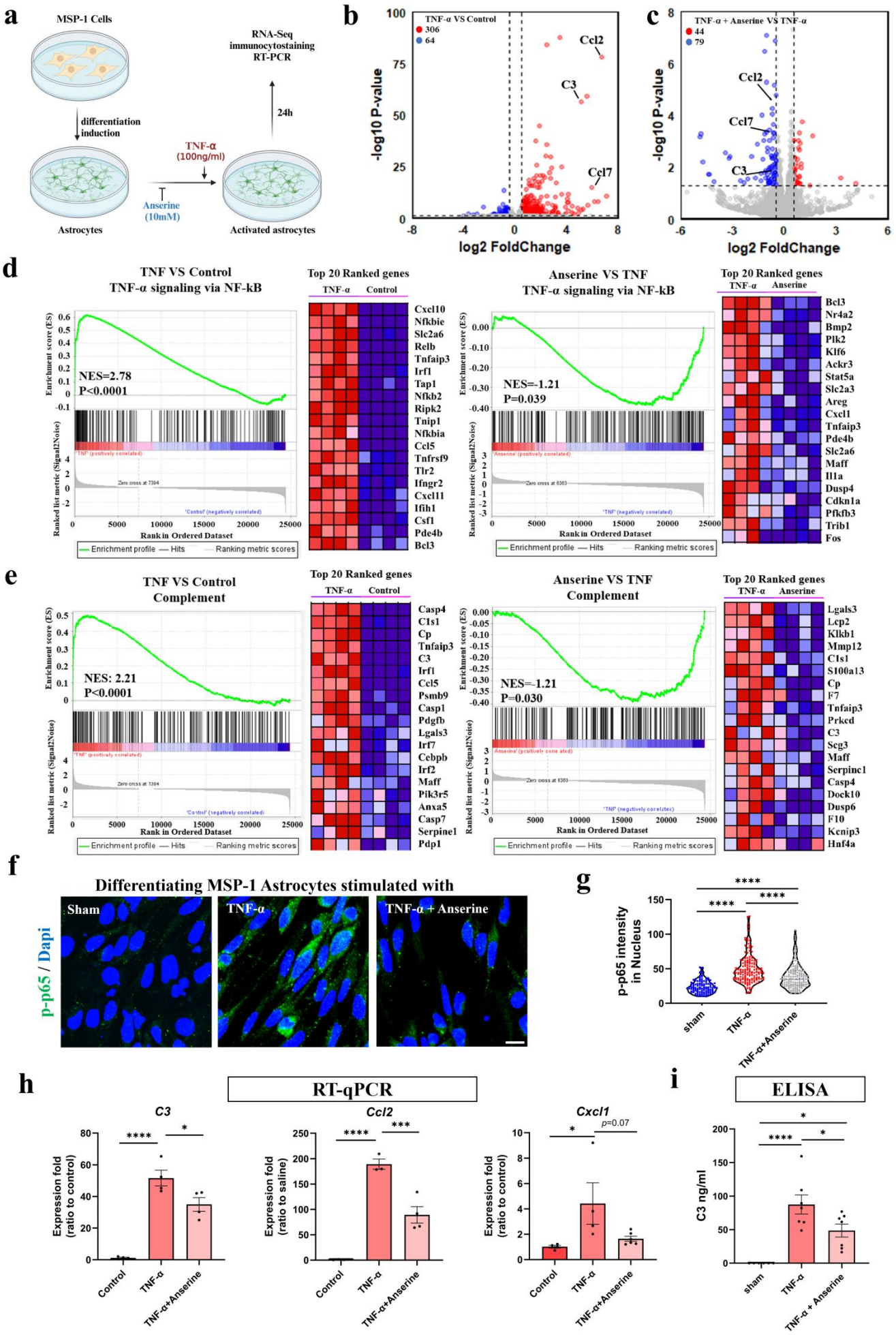
a
MSP-1 Cells
differentiation induction
Astrocytes
TNF-α (100ng/ml)
Anserine (10mM)
24h
RNA-Seq immunocytostaining RT-PCR
Activated astrocytes
b
TNF-α VS Control
306
64
Ccl2
C3
Ccl7
-log10 P-value
log2 FoldChange
c
TNF-α + Anserine VS TNF-α
44
79
Ccl2
Ccl7
C3
-log10 P-value
log2 FoldChange
d
TNF VS Control
TNF-α signaling via NF-kB
NES=2.78
P<0.0001
Top 20 Ranked genes
TNF-α
Control
Cxcl10
Nfkbie
Slc2a6
Relb
Tnfaip3
Irf1
Tap1
Nfkb2
Ripk2
Tnip1
Nfkbia
Ccl5
Tnfrsf9
Tlr2
Ifngr2
Cxcl11
Ifih1
Csf1
Pde4b
Bcl3
Anserine VS TNF
TNF-α signaling via NF-kB
NES=-1.21
P=0.039
Top 20 Ranked genes
TNF-α
Anserine
Bcl3
Nr4a2
Bmp2
Plk2
Klf6
Ackr3
Stat5a
Slc2a3
Areg
Cxcl1
Tnfaip3
Pde4b
Slc2a6
Maff
Il1a
Dusp4
Cdkn1a
Pfkfb3
Trib1
Fos
Enrichment score (ES)
Ranked list metric (Signal2Noise)
Rank in Ordered Dataset
Enrichment profile
Hits
Ranking metric scores
e
TNF VS Control
Complement
NES: 2.21
P<0.0001
Top 20 Ranked genes
TNF-α
Control
Casp4
C1s1
Cp
Tnfaip3
C3
Irf1
Ccl5
Psmb9
Casp1
Pdgfb
Lgals3
Irf7
Cebpb
Irf2
Maff
Pik3r5
Anxa5
Casp7
Serpine1
Pdp1
Anserine VS TNF
Complement
NES=-1.21
P=0.030
Top 20 Ranked genes
TNF-α
Anserine
Lgals3
Lcp2
Klkb1
Mmp12
C1s1
S100a13
Cp
F7
Tnfaip3
Prkcd
C3
Scg3
Maff
Serpinc1
Casp4
Dock10
Dusp6
F10
Kcnip3
Hnf4a
f
Differentiating MSP-1 Astrocytes stimulated with
Sham
TNF-α
TNF-α + Anserine
p-p65 / Dapi
g
p-p65 intensity in Nucleus
sham
TNF-α
TNF-α+Anserine
h
RT-qPCR
C3
Ccl2
Cxcl1
p=0.07
Expression fold (ratio to control)
Expression fold (ratio to saline)
Control
TNF-α
TNF-α+Anserine
i
ELISA
C3 ng/ml
sham
TNF-α
TNF-α + Anserine

Fig. 1 Anserine suppressed astrocyte activation and C3 over-production in MPS-1 astrocytes.
a Brief description of in vitro study using Mouse striatal precursor-1 (MSP-1) cells differentiation-induced astrocytes. Before TNF-α (100ng/ml) treatment, 10μM anserine was added into the medium for 2 hours. TNF-α treatment was performed within 24 hours. **b** and **c** Volcano plot of identified DEGs (|log2 Foldchange|> 0.5, $p < 0.05$, up, red, down, blue) between TNF-α group and Control group (**b**) or Anserine + TNF-α group and TNF-α group (**c**). **d** The result of GESA using the Hallmark database, focused on the complement system. **e** The result of GESA using the Hallmark database, focused on the NF-κB pathway. **f** Representative images of p-p65 staining in MSP-1 astrocytes of control, TNF-α and Anserine + TNF-α group (scale bar: 10 μm). **g** Quantification of p-p65 intensity in the nucleus of 3 groups, (n=110-152). **h** Quantification of *C3*, *Ccl2* and *Cxcl1* expression of 3 groups, (n=3-6). **f** Result of C3 concentration in cultured medium of control, TNF-α and Anserine + TNF-α group, (n=6-7). Data represent means ± SEM and were analyzed by one-way ANOVA with Tukey's multiple comparisons test. *$p < 0.05$, ***$p < 0.001$, ****$p < 0.0001$.

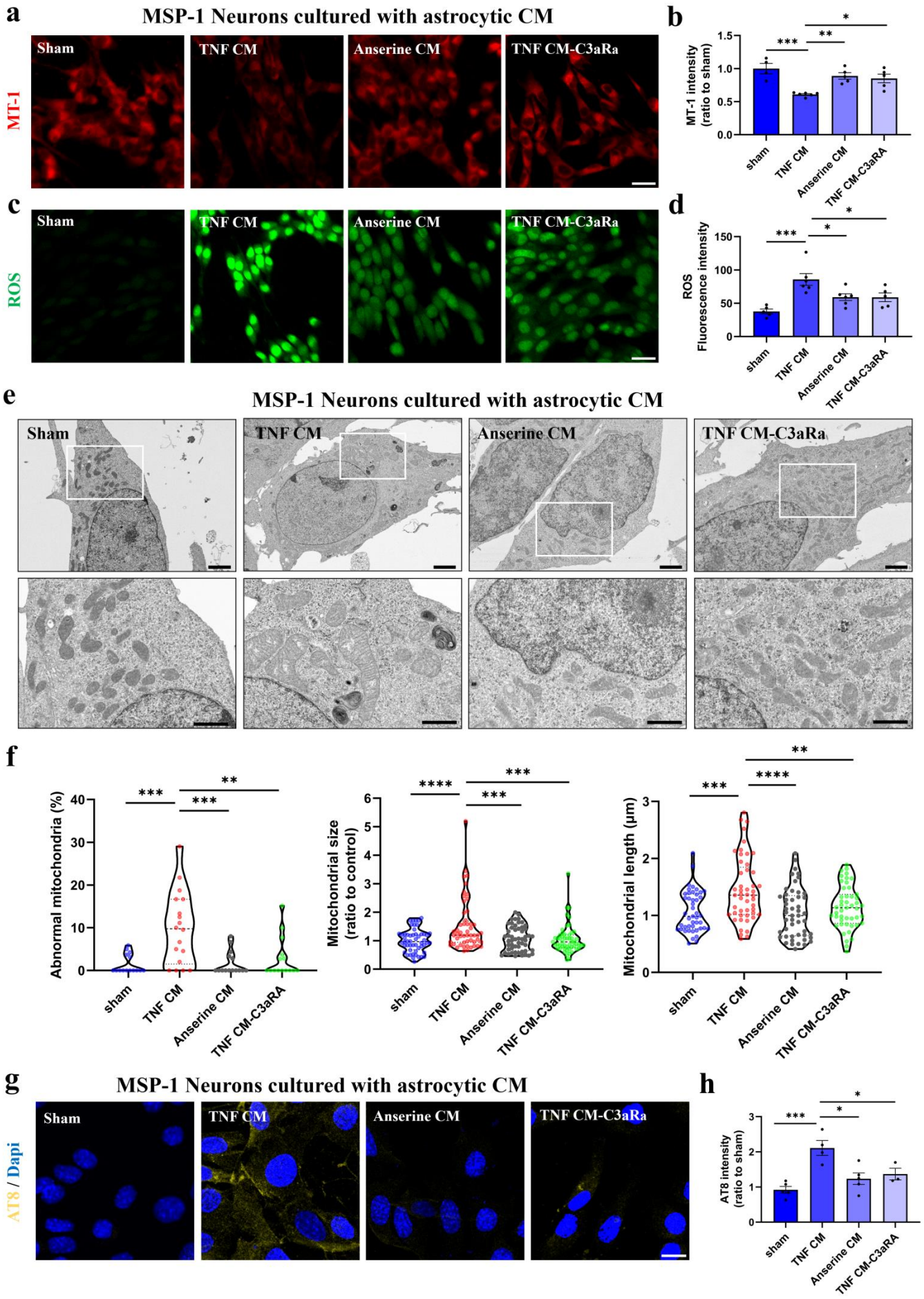
a
MSP-1 Neurons cultured with astrocytic CM
MT-1
Sham
TNF CM
Anserine CM
TNF CM-C3aRa
b
MT-1 intensity (ratio to sham)
sham
TNF CM
Anserine CM
TNF CM-C3aRA
c
ROS
d
ROS Fluorescence intensity
e
MSP-1 Neurons cultured with astrocytic CM
f
Abnormal mitochondria (%)
Mitochondrial size (ratio to control)
Mitochondrial length (μm)
g
MSP-1 Neurons cultured with astrocytic CM
AT8 / Dapi
h
AT8 intensity (ratio to sham)

Fig. 2 Downregulation of astrocytic C3 production alleviated tau-mediated neuronal mitochondrial dysfunction in MSP-1 neurons.

a Representative images of MT-1 staining of MSP-1 neurons treated with sham, TNF CM, Anserine CM and TNF CM-C3aRA (10μM) (scale bar: 25 μm). **b** Quantification of MT-1 intensity in each group, (n=4-6). c Representative images of ROS staining of MSP-1 neurons treated with sham, TNF CM, Anserine CM and TNF CM-C3aRA (10μM) (scale bar: 25 μm). **d** Quantification of ROS fluorescence intensity in each group, (n=5-6). **e** Representative electron microscopic images of MSP-1 neurons treated with sham, TNF CM, Anserine CM and TNF CM-C3aRA (scale bar: 2 μm (up), 1 μm (down)). **f** Quantification of abnormal mitochondria, mitochondrial size and mitochondrial length in each group (n=15-53). **g** Representative images of AT8 staining of MSP-1 neurons treated with sham, TNF CM, Anserine CM and TNF CM-C3aRA (10μM) (scale bar: 10 μm). **h** Quantification of AT8 intensity in each group, (n=3-5). Data represent means ± SEM and were analyzed by one-way ANOVA with Tukey's multiple comparisons test. *$p < 0.05$, **$p < 0.01$, ***$p < 0.001$, ****$p < 0.0001$.

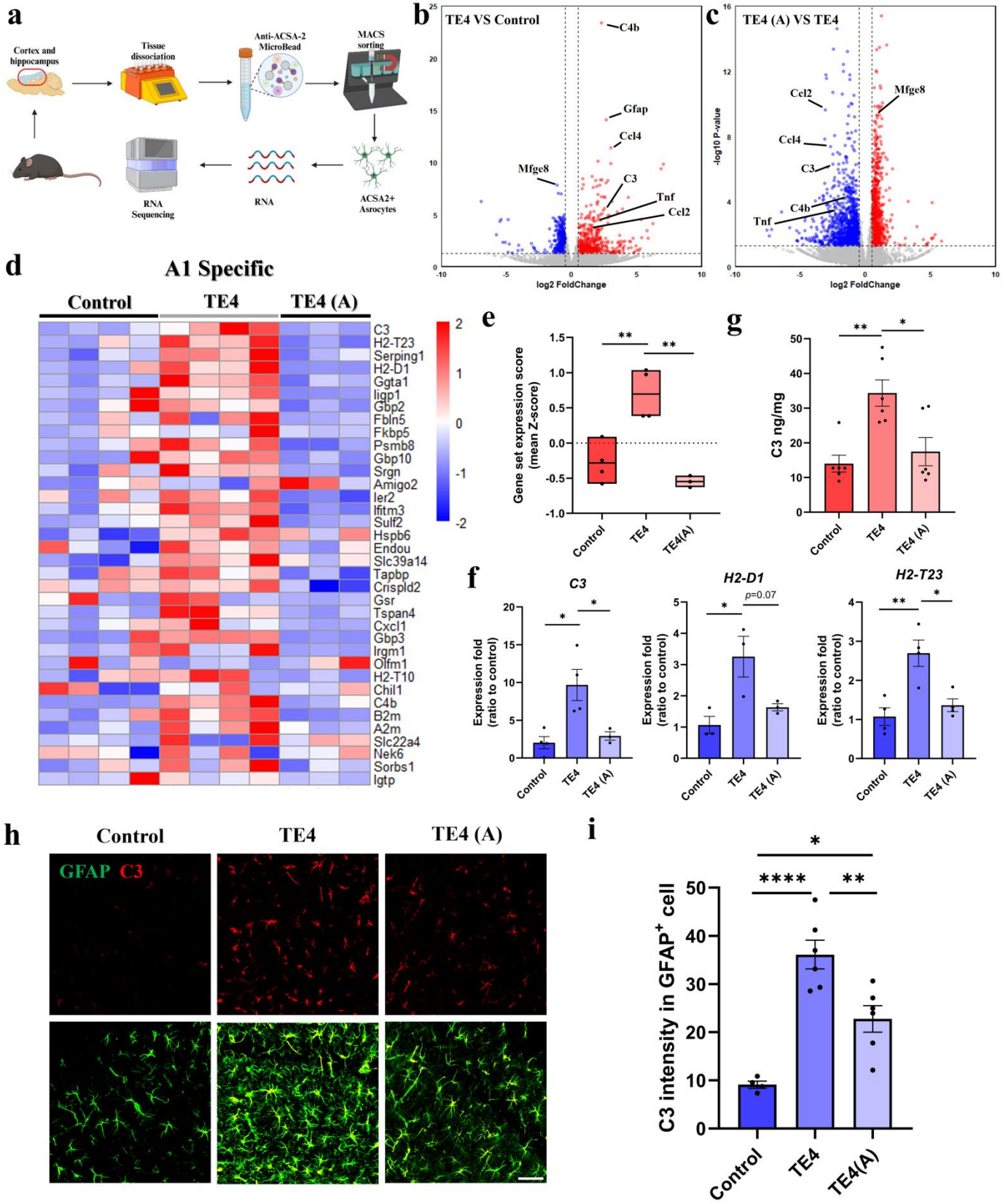
a
Cortex and hippocampus
Tissue dissociation
Anti-ACSA-2 MicroBead
MACS sorting
ACSA2+ Asrocytes
RNA
RNA Sequencing
b
TE4 VS Control
C4b
Gfap
Ccl4
Mfge8
C3
Tnf
Ccl2
log2 FoldChange
c
TE4 (A) VS TE4
Ccl2
Mfge8
Ccl4
C3
C4b
Tnf
-log10 P-value
log2 FoldChange
d
A1 Specific
Control
TE4
TE4 (A)
C3
H2-T23
Serping1
H2-D1
Ggta1
Iigp1
Gbp2
Fbln5
Fkbp5
Psmb8
Gbp10
Srgn
Amigo2
Ier2
Ifitm3
Sulf2
Hspb6
Endou
Slc39a14
Tapbp
Crispld2
Gsr
Tspan4
Cxcl1
Gbp3
Irgm1
Olfm1
H2-T10
Chil1
C4b
B2m
A2m
Slc22a4
Nek6
Sorbs1
Igtp
e
Gene set expression score (mean Z-score)
Control
TE4
TE4(A)
g
C3 ng/mg
Control
TE4
TE4 (A)
f
C3
H2-D1
p=0.07
H2-T23
Expression fold (ratio to control)
Control
TE4
TE4 (A)
h
Control
TE4
TE4 (A)
GFAP C3
i
C3 intensity in GFAP+ cell
Control
TE4
TE4(A)

Fig. 3 Anserine treatment suppressed A1 astrocyte activation and C3 over-production in TE4 tauopathy model mice.

a The description of astrocytes isolation for RNA-Seq used ACSA-2 Microbead from mouse brain. **b** and **c** Volcano plot of identified DEGs (|log2 Foldchange|>1, $p<0.05$, up, red, down, blue) between astrocytes of TE4 mice and Control mice (**b)** or between astrocytes of TE4 (A) mice and TE4 mice (**c**). **d** Heatmap that shows expression levels of selected A1 specific markers in control, TE4 and TE4 (A) mice. **e** Quantification of gene set expression score of A1 specific astrocytes markers and TPM expression data of selected A1 astrocytes genes in each group and (n=4). **f** RT-qPCR results of the expression of *C3*, *H2-D1* and *H2-T23* in each group (n=3-4). **g** Results of C3 concentration in hippocampus of 3 groups of mice, (n=6). **h** Representative images of GFAP and C3 co-staining in the hippocampus area of 3 groups of mice (scale bar: 50 μm). **i** Quantification of C3 intensity in GFAP positive cells in each group, (n=4-6). Data represent means ± SEM and were analyzed by one-way ANOVA with Tukey's multiple comparisons test. *$p < 0.05$, **$p < 0.01$, ***$p < 0.001$, ****$p < 0.0001$

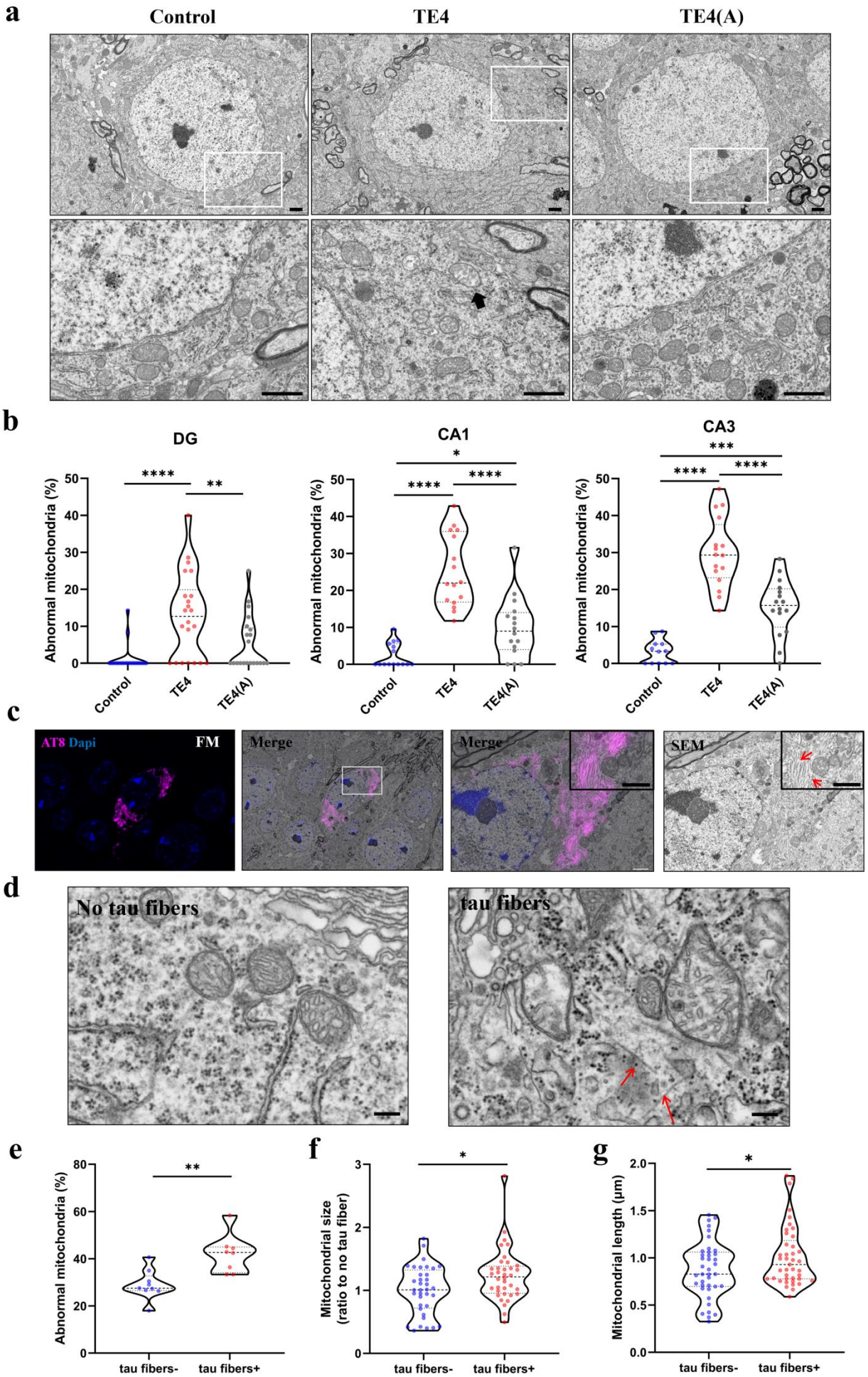
a
Control
TE4
TE4(A)
b
DG
CA1
CA3
Abnormal mitochondria (%)
Control
TE4
TE4(A)
c
AT8 Dapi
FM
Merge
Merge
SEM
d
No tau fibers
tau fibers
e
Abnormal mitochondria (%)
tau fibers-
tau fibers+
f
Mitochondrial size
(ratio to no tau fiber)
tau fibers-
tau fibers+
g
Mitochondrial length (μm)
tau fibers-
tau fibers+

Fig. 4 Downregulation of astrocytic C3 production alleviated mitochondrial dysfunction mediated by tau pathology in TE4 mice.

a Representative electron microscopic images of hippocampal neurons in control, TE4 and TE4 (A) mice (scale bar: 1 μm). Neurons that in TE4 mice showed increased abnormal mitochondria with swollen structures (black arrow). **b** Quantification of abnormal mitochondria in DG, CA1 and CA3 area of 3 groups of mice (n=12-22). **c** Representative of CLEM images of AT8 positive neurons in TE4 mice hippocampus area. The red arrow showed the tau fibers aggregated in the cell body (scale bar: 1 μm). **d** Representative SEM images of neurons contained tau fibers and neurons contained no tau fibers in TE4 mice (scale bar: 0.5 μm). **e** Quantification of abnormal mitochondria in neurons with no tau fibers and fibers in TE4 mice hippocampus area, (n=8-9). **f** Quantification of mitochondrial size in neurons with no tau fibers and fibers in TE4 mice hippocampus area, (n=36). **g** Quantification of mitochondrial length in neurons with tau fibers and no tau fibers of TE4 mice, (n=39-41). Data represent means ± SEM and were analyzed by Student's t-test (**e, f and g**) and one-way ANOVA with Tukey's multiple comparisons test (**b**). *$p < 0.05$, **$p < 0.01$, ***$p < 0.001$, ****$p < 0.0001$.

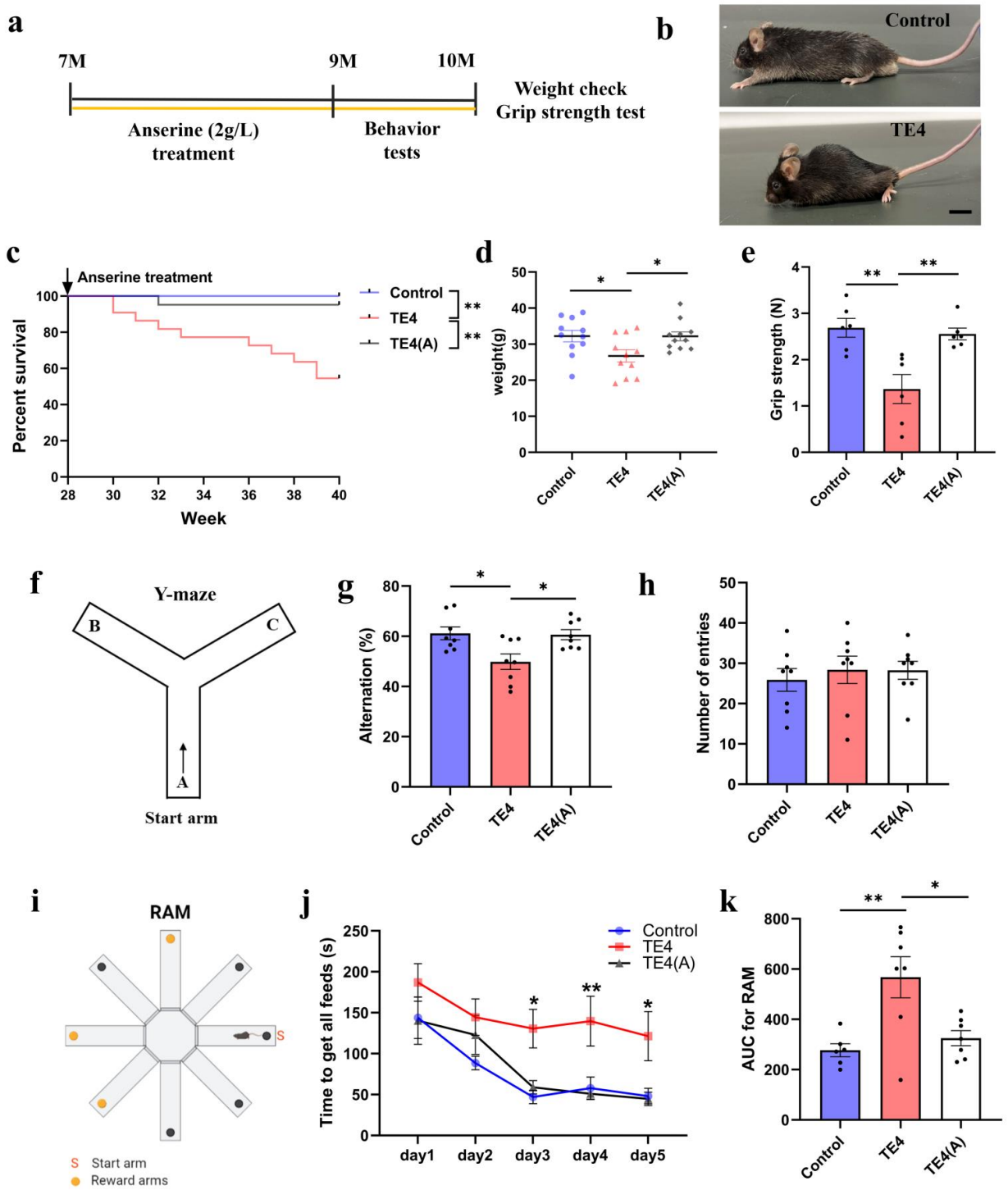

Fig. 5 Prolonged the survival rate, reversed physiological deficits and improved cognitive function in anserine-treated TE4 mice.

a Description of behavior experiments and physiological function check. **b** Representative images of control mice and TE4 mice (scale bar: 1 cm). **c** Kaplan-Meier survival analysis of control, TE4 and TE4 (A) groups, (n=15-22). **d** Quantification of body weight of 3 groups of mice at the end of behavior tests, (n=11). **e** Quantification of grip strength of 3 groups of mice at the end of behavior tests, (n=6). **f** Description of Y-Maze, the mouse would start at A site. **g** and **h** Results of Y-maze. The results were presented as alternation rates (%) (**g**) and the number of entries (**h**) in the Y-maze of 3 groups of mice during 10 min, (n=8). **i** Description of Radial arm maze (RAM). **j** and **k** Results of RAM. The time of cost to find all the feeds was recorded (**j**) in a 5-days RAM test. At the same time, the area of the time curve for the 5-day RAM test was calculated for each mouse (**k**) (n=6-7). Data represent means ± SEM and were analyzed by one-way ANOVA with Tukey's multiple comparisons test (**d**, **e**, **g**, **h**, and **k**) or two-way repeated ANOVA with Tukey's multiple comparisons test (**j**). *$p < 0.05$, **$p < 0.01$.

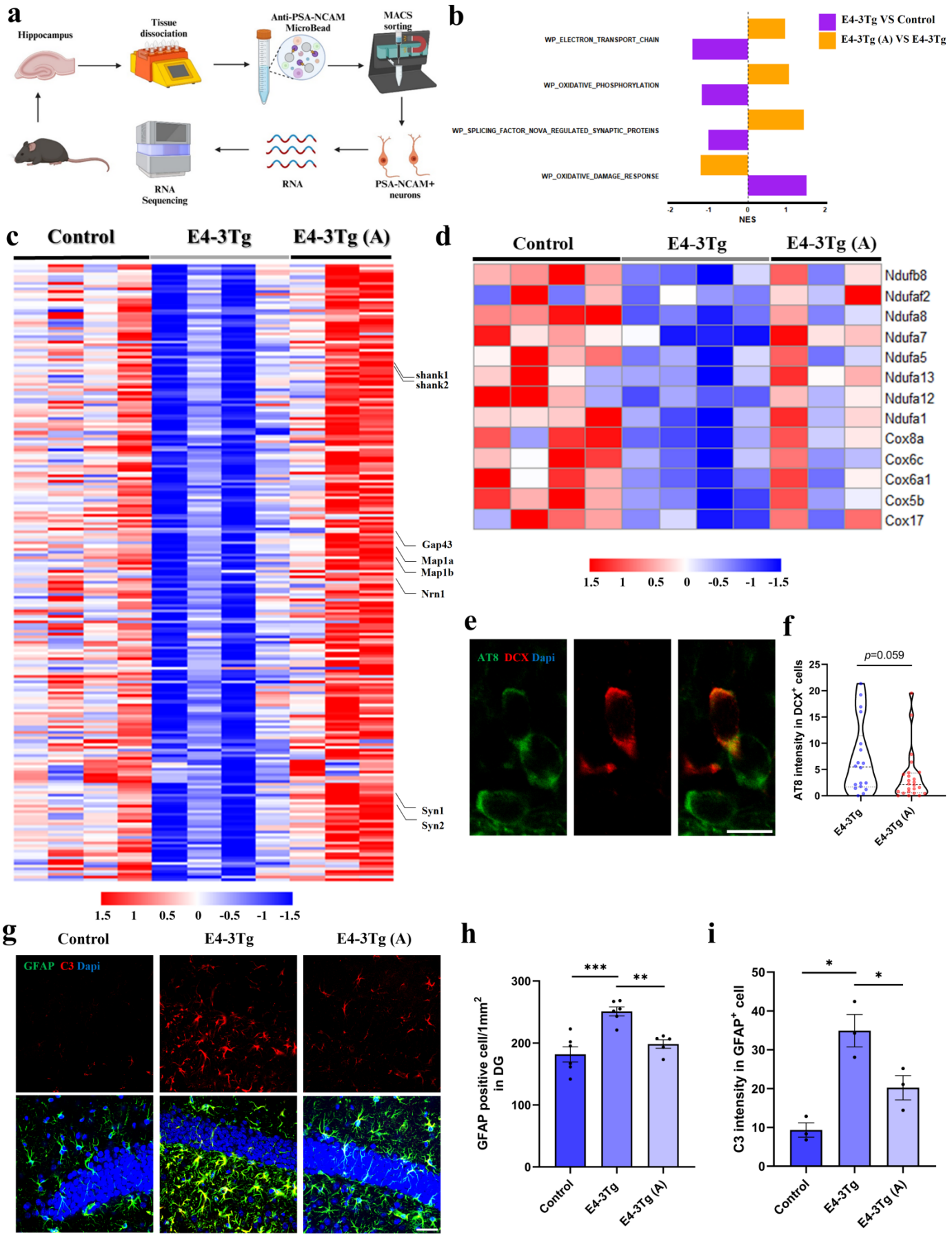
a
Hippocampus
Tissue dissociation
Anti-PSA-NCAM MicroBead
MACS sorting
PSA-NCAM+ neurons
RNA
RNA Sequencing
b
E4-3Tg VS Control
E4-3Tg (A) VS E4-3Tg
WP_ELECTRON_TRANSPORT_CHAIN
WP_OXIDATIVE_PHOSPHORYLATION
WP_SPLICING_FACTOR_NOVA_REGULATED_SYNAPTIC_PROTEINS
WP_OXIDATIVE_DAMAGE_RESPONSE
NES
c
Control
E4-3Tg
E4-3Tg (A)
shank1
shank2
Gap43
Map1a
Map1b
Nrn1
Syn1
Syn2
1.5 1 0.5 0 -0.5 -1 -1.5
d
Control
E4-3Tg
E4-3Tg (A)
Ndufb8
Ndufaf2
Ndufa8
Ndufa7
Ndufa5
Ndufa13
Ndufa12
Ndufa1
Cox8a
Cox6c
Cox6a1
Cox5b
Cox17
1.5 1 0.5 0 -0.5 -1 -1.5
e
AT8 DCX Dapi
f
p=0.059
AT8 intensity in DCX+ cells
E4-3Tg
E4-3Tg (A)
g
Control
E4-3Tg
E4-3Tg (A)
GFAP C3 Dapi
h
GFAP positive cell/1mm2 in DG
***
**
Control
E4-3Tg
E4-3Tg (A)
i
C3 intensity in GFAP+ cell
*
*
Control
E4-3Tg
E4-3Tg (A)

Fig. 6 Downregulation of astrocytic C3 secretion alleviated synapse impairment and mitochondrial dysfunction in newborn neurons in E4-3Tg model mice.

a Brief description of newborn neuron isolation for RNA-Seq used PSA-NCAM Microbead from mouse hippocampus. **b** Representative GESA results using the Wiki Pathway database focused on mitochondrial function. Purple, E4-3Tg VS control. Orange, E4-3Tg (A) VS E4-3Tg. **c** and **d** Heatmap that shows expression levels of synapse (**c**) and mitochondria markers (**d**) of 3 groups of mice. All the selected genes were significantly down-regulated in E4-3Tg group and up-regulated in E4-3Tg (A) group. **e** Representative images of DCX and AT8 co-staining in DG area of E4-3Tg mice and E4-3Tg (A) mice (scale bar: 10 μm). **f** Quantification of AT8 intensity in DCX positive cells of each group, (n=18-24). **g** Representative images of GFAP and C3 co-staining in DG area of control, E4-3Tg and E4-3Tg (A) mice (scale bar: 25 μm). **h** Quantification of the number of GFAP positive cells in DG area of each group, (n=5-6). **i** Quantification of C3 intensity in GFAP positive cells in each group, (n=3). Data represent means ± SEM and were analyzed by Student's t-test (**f**) and one-way ANOVA with Tukey's multiple comparisons test (**h** and **i**). *$p < 0.05$, **$p < 0.01$.

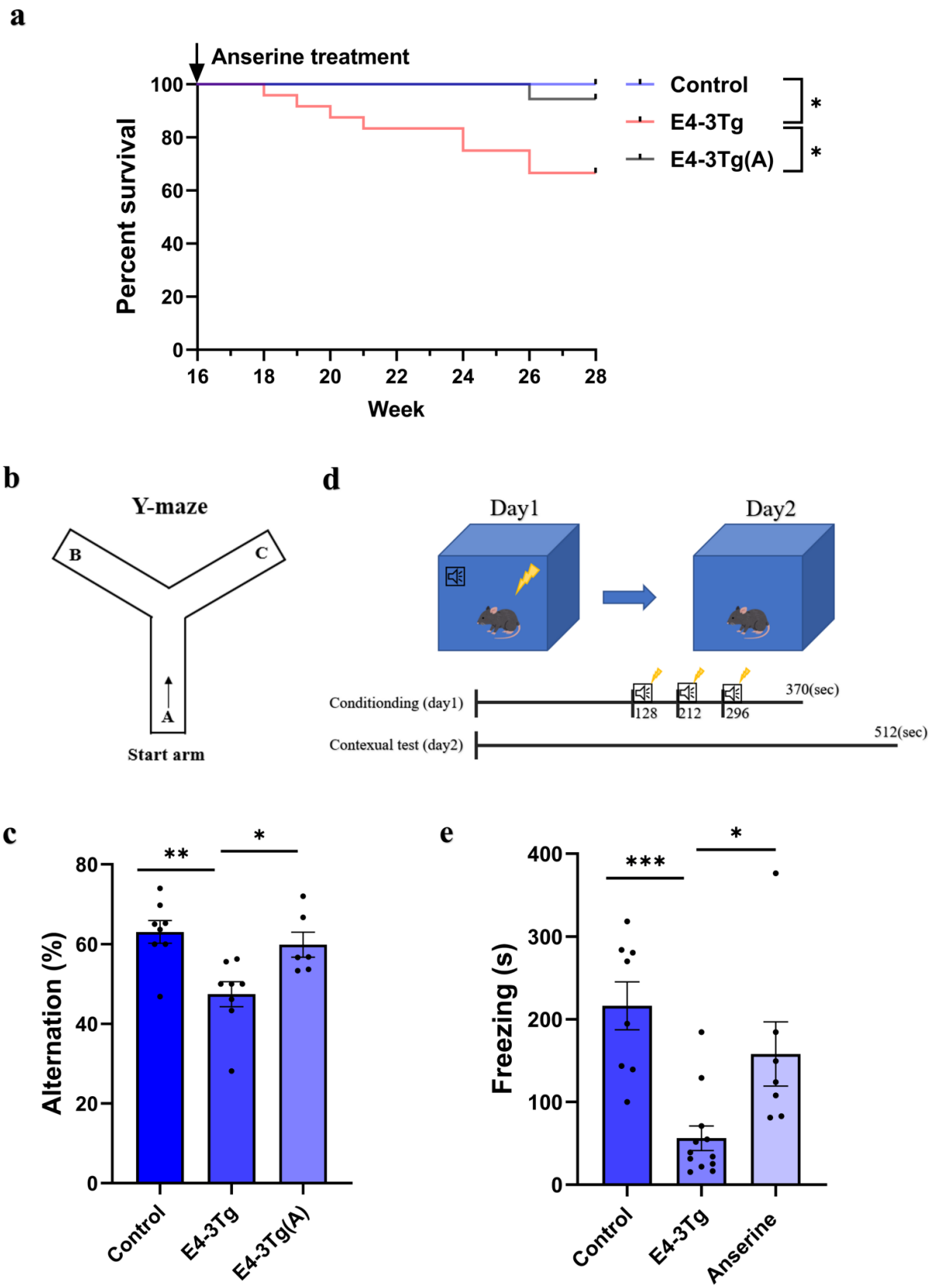

Fig. 7 Improved AHN rescued the cognitive function in E4-3Tg mice.
a Kaplan–Meier survival analysis of control, TE4 and TE4 (A) groups, (n=12-24). **b** Description of Y-Maze, mice would start at A site. **c** Result of Y-maze. The result was presented as alternation rates (%) of each group of mice during 10 min, (n=6-8). **d** Description of CFC test. **e** Quantification of Freezing time in each group at contextual test, (n=7-12). Data represent means ± SEM and were analyzed by one-way ANOVA with Tukey's multiple comparisons test. *$p < 0.05$, **$p < 0.01$, ***$p < 0.001$.

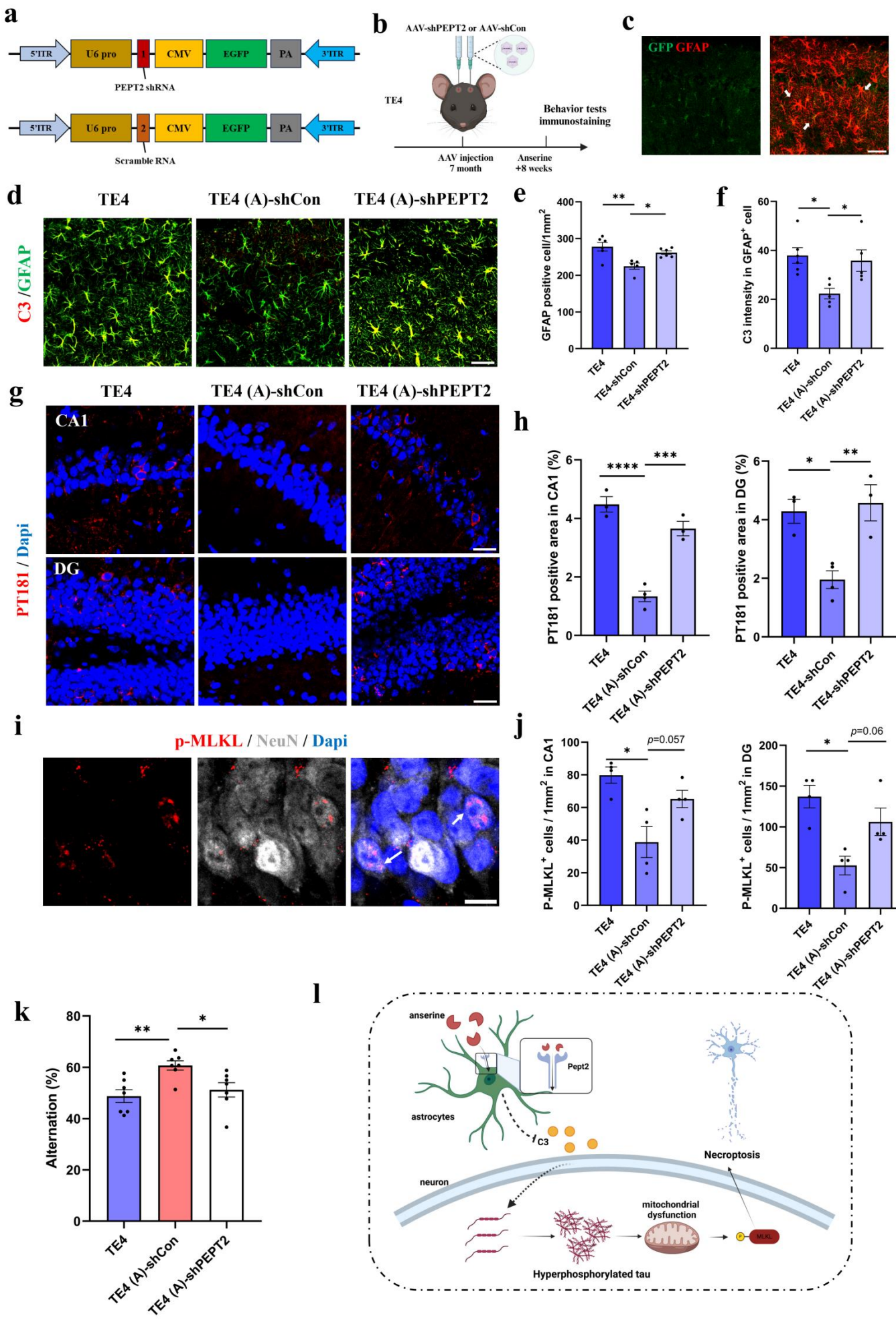
a
5'ITR
U6 pro
1
CMV
EGFP
PA
3'ITR
PEPT2 shRNA
2
Scramble RNA
b
AAV-shPEPT2 or AAV-shCon
TE4
Behavior tests
immunostaining
AAV injection
7 month
Anserine
+8 weeks
c
GFP GFAP
d
TE4
TE4 (A)-shCon
TE4 (A)-shPEPT2
C3 /GFAP
e
GFAP positive cell/1mm²
TE4
TE4-shCon
TE4-shPEPT2
f
C3 intensity in GFAP⁺ cell
TE4 (A)-shCon
TE4 (A)-shPEPT2
g
CA1
DG
PT181 / Dapi
h
PT181 positive area in CA1 (%)
PT181 positive area in DG (%)
i
p-MLKL / NeuN / Dapi
j
P-MLKL⁺ cells / 1mm² in CA1
P-MLKL⁺ cells / 1mm² in DG
p=0.057
p=0.06
k
Alternation (%)
l
anserine
Pept2
astrocytes
C3
Necroptosis
neuron
mitochondrial
dysfunction
MLKL
Hyperphosphorylated tau

Fig. 8 Knockdown of anserine transporter blocked the effects of anserine on downregulating astrocytic C3 production

a and **b** The description of AAV experiment. **c** Representative images of GFAP and GFP co-staining in the hippocampus area of AAV-injected TE4 mice (scale bar: 50 μm). **d** Representative images of GFAP and C3 co-staining in Hippocampus area in TE4, TE4 (A)-shCon and TE4 (A)-shPept2 mice (scale bar: 50 μm). **e** Quantification of the number of GFAP positive cells in each group, (n=5-6). **f** Quantification of C3 intensity in GFAP positive cells in each group, (n=5-6). **f** Representative images of PT181 staining in hippocampal CA1 and DG area in TE4, TE4 (A)-shCon and TE4 (A)-shPept2 mice (scale bar: 25 μm). **g** Quantification of PT181 positive stain area in each group, (n=3-4). **i** Representative images of p-MLKL and NeuN co-staining in TE4 mice (scale bar: 10 μm). **j** Quantification of p-MLKL positive neurons in CA1 and DG area in each group, (n=4). **k** Result of Y-maze in TE4, TE4 (A)-shCon and TE4 (A)-shPept2 mice, (n=7). **l** Brief diagram about the mechanism of anserine suppressing astrocyte activation. Data represent means ± SEM and were analyzed by one-way ANOVA with Tukey's multiple comparisons test. *$p < 0.05$, **$p < 0.01$, ***$p < 0.001$, ****$p < 0.0001$.

Supplementary Figure

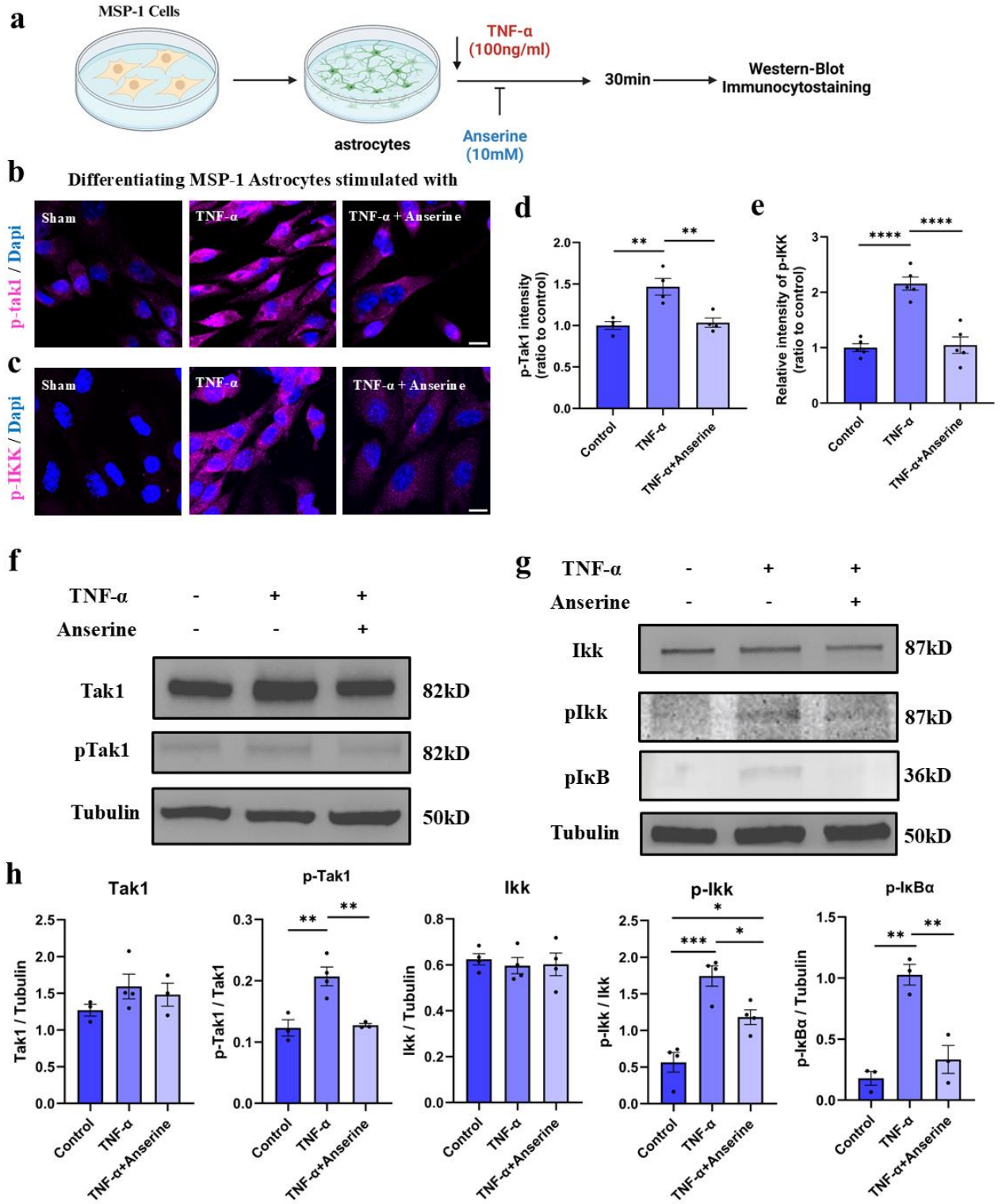

Supplementary Fig. 1 Anserine inhibited the activation of Tak1 to suppress the activation of NF-κB pathway.

a Brief description of experiment to study the mechanism of anserine on suppressing NF-κB activity. 10μM anserine was added into the medium for 2 hours. TNF-α treatment was performed within 30 min. **b** and **c** Representative image of p-Tak1 (**b**) and p-Ikk (**c**) staining in MSP-1 astrocytes (scale bar: 10 μm). **d** and **e** Quantification of p-Tak1 (**d**) and p-Ikk (**e**) intensity in each group, (n=4-5). **f** Representative western blot images of Tak1 and p-Tak1 in MSP-1 astrocytes of each group. **g** Representative western blot images of IKK, p-IKK and p-IκBα in each group. **h** Quantification of relative expression in each group, (n=3-4). Data represent means ± SEM and were analyzed by one-way ANOVA with Tukey's multiple comparisons test. *$p < 0.05$, **$p < 0.01$, ***$p < 0.001$, ****$p<0.0001$.

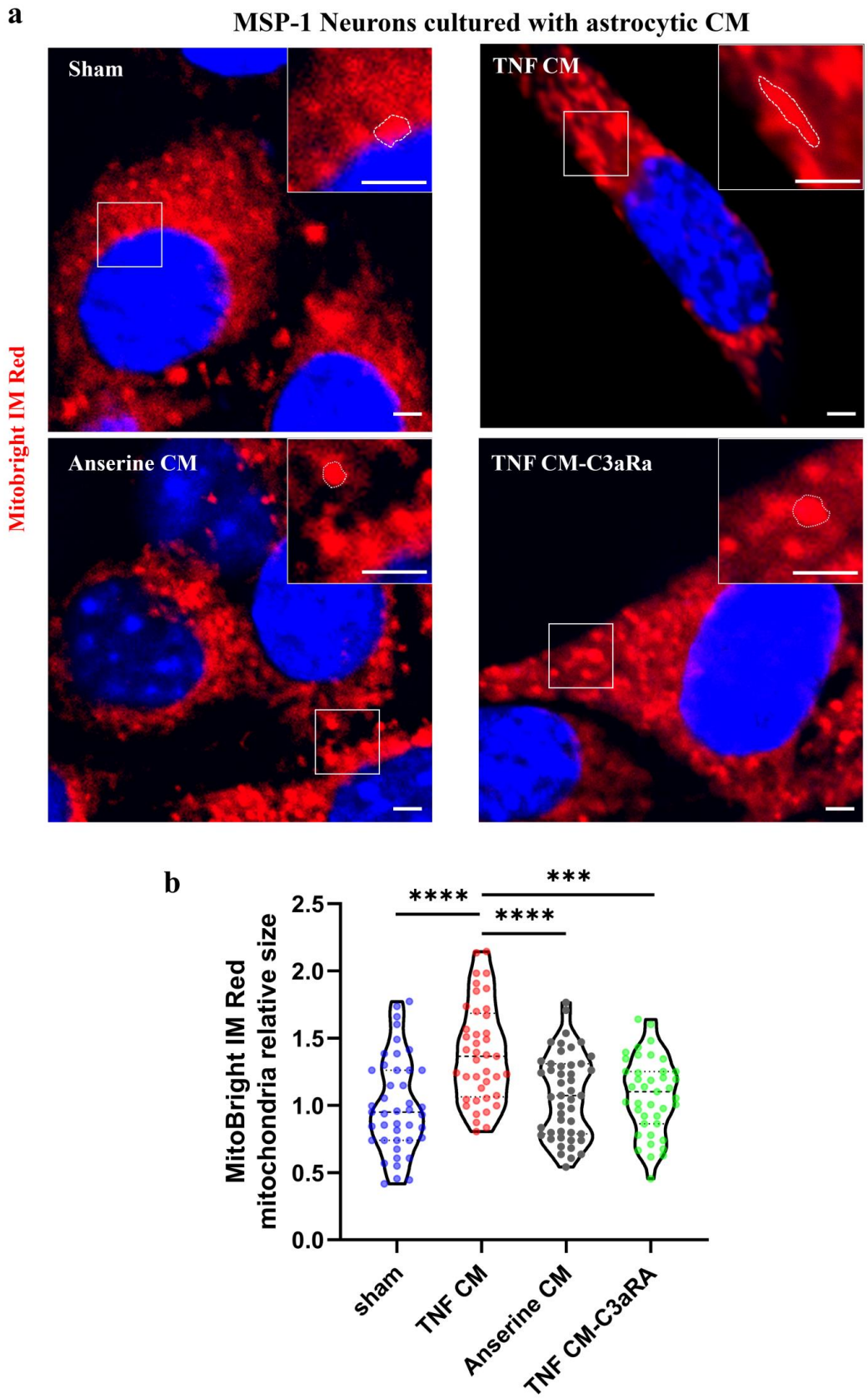

Supplementary Fig. 2 Downregulation of astrocytic C3 production alleviated mitochondrial swelling in MSP-1 neurons.

a Representative images of MSP-1 neurons stained with Mitobright IM Red (scale bar: 2 μm). **b** Quantification of mitochondrial size of each group (n=41-47). Data represent means ± SEM and were analyzed by one-way ANOVA with Tukey's multiple comparisons test. ***$p < 0.001$, ****$p < 0.0001$.

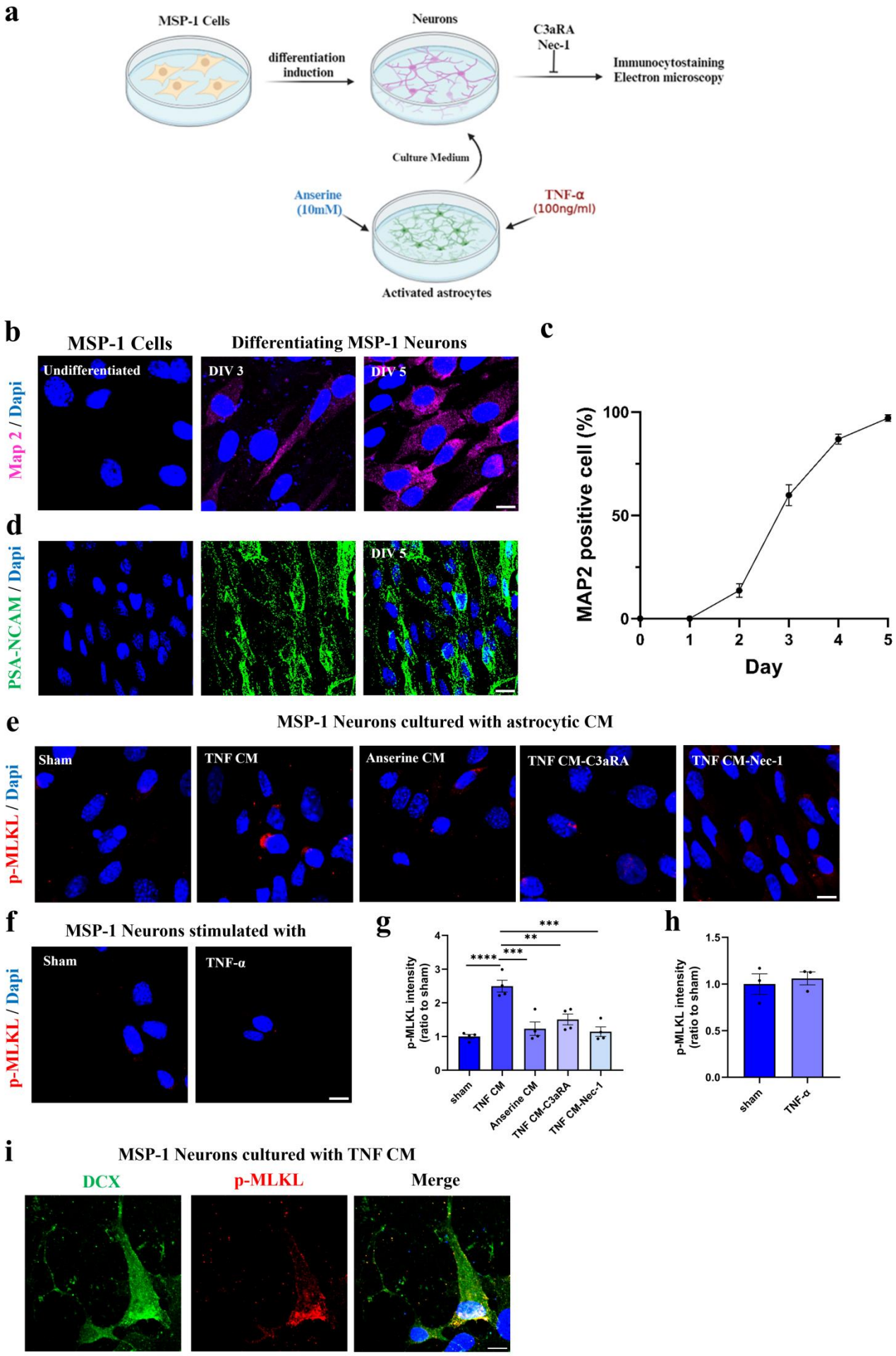
a
MSP-1 Cells
differentiation induction
Neurons
C3aRA
Nec-1
Immunocytostaining
Electron microscopy
Culture Medium
Anserine (10mM)
TNF-α (100ng/ml)
Activated astrocytes
b
MSP-1 Cells
Differentiating MSP-1 Neurons
Undifferentiated
DIV 3
DIV 5
Map 2 / Dapi
c
MAP2 positive cell (%)
Day
d
PSA-NCAM / Dapi
DIV 5
e
MSP-1 Neurons cultured with astrocytic CM
Sham
TNF CM
Anserine CM
TNF CM-C3aRA
TNF CM-Nec-1
p-MLKL / Dapi
f
MSP-1 Neurons stimulated with
Sham
TNF-α
p-MLKL / Dapi
g
p-MLKL intensity (ratio to sham)
sham
TNF CM
Anserine CM
TNF CM-C3aRA
TNF CM-Nec-1
h
p-MLKL intensity (ratio to sham)
sham
TNF-α
i
MSP-1 Neurons cultured with TNF CM
DCX
p-MLKL
Merge

Supplementary Fig. 3 Suppressed astrocytic C3 production by anserine prevented necroptosis activation in MSP-1 neurons

a Brief description of in vitro study using MSP-1 cells differentiation-induced neurons. MSP-1 neurons were treated with collected Cultured medium (CM) from MSP-1 astrocytes for 24 hours. **b** Representative images of MAP2 staining during the neuron-differentiation of MSP-1 cells (scale bar: 10 μm). **c** Quantification of MAP2 positive cells ratio during DIV0-DIV5, (n=3). **d** Representative images of PSA-NCAM staining in MSP-1 neurons at DIV5 (scale bar: 25 μm). **e** Representative images of p-MLKL staining of MSP-1 neurons treated with sham, TNF CM and Anserine CM, TNF CM-C3aRA (10μM) and TNF CM-Nec-1 (30μM) (scale bar: 10 μm). **f** Representative images of p-MLKL staining in MSP-1 neurons treated with sham or TNF-α (100ng/ml) (scale bar: 10 μm). **g** and **h** Quantification of p-MLKL staining in each group, (n=3-4). **i** Representative images of DCX and p-MLKL co-staining in MSP-1 neurons treated with TNF CM (scale bar: 10 μm). Data represent means ± SEM and were analyzed by Student's t-test (**h**) and one-way ANOVA with Tukey's multiple comparisons test (**g**). $^{**}p < 0.01$, $^{***}p < 0.001$, $^{****}p < 0.0001$.

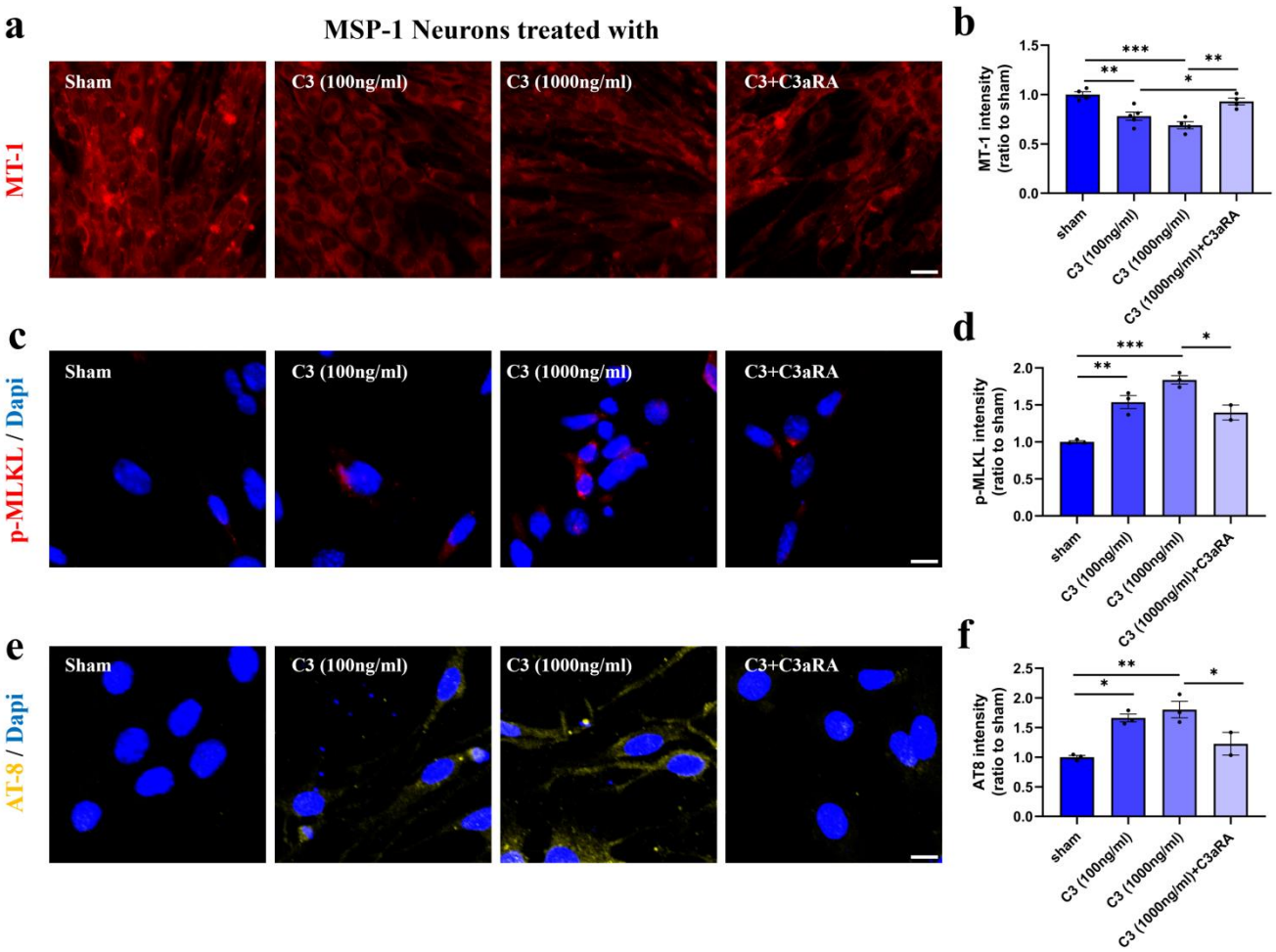

Supplementary Fig. 4 Complement C3 triggered tau-mediated mitochondrial dysfunction and necroptosis activation in MSP-1 neurons.

a Representative images of MT-1 staining of MSP-1 neurons treated with sham, C3 (100ng/ml), C3 (1000ng/ml) and C3-C3aRA (10μM) (scale bar: 25 μm). **b** Quantification of MT-1 intensity in each group, (n=4-5). **c** Representative images of p-MLKL staining of MSP-1 neurons treated with sham, C3 (100ng/ml), C3 (1000ng/ml) and C3-C3aRA (10μM) (scale bar: 10 μm) **d** Quantification of p-MLKL intensity in each group, (n=3-4). **e** Representative images of AT8 staining of MSP-1 neurons treated with sham, C3 (100ng/ml), C3 (1000ng/ml) and C3-C3aRA (10μM) (scale bar: 10 μm). **f** Quantification of AT8 intensity in each group, (n=3-4). Data represent means ± SEM and were analyzed by one-way ANOVA with Tukey's multiple comparisons test. *$p < 0.05$, **$p < 0.01$, ***$p < 0.001$.

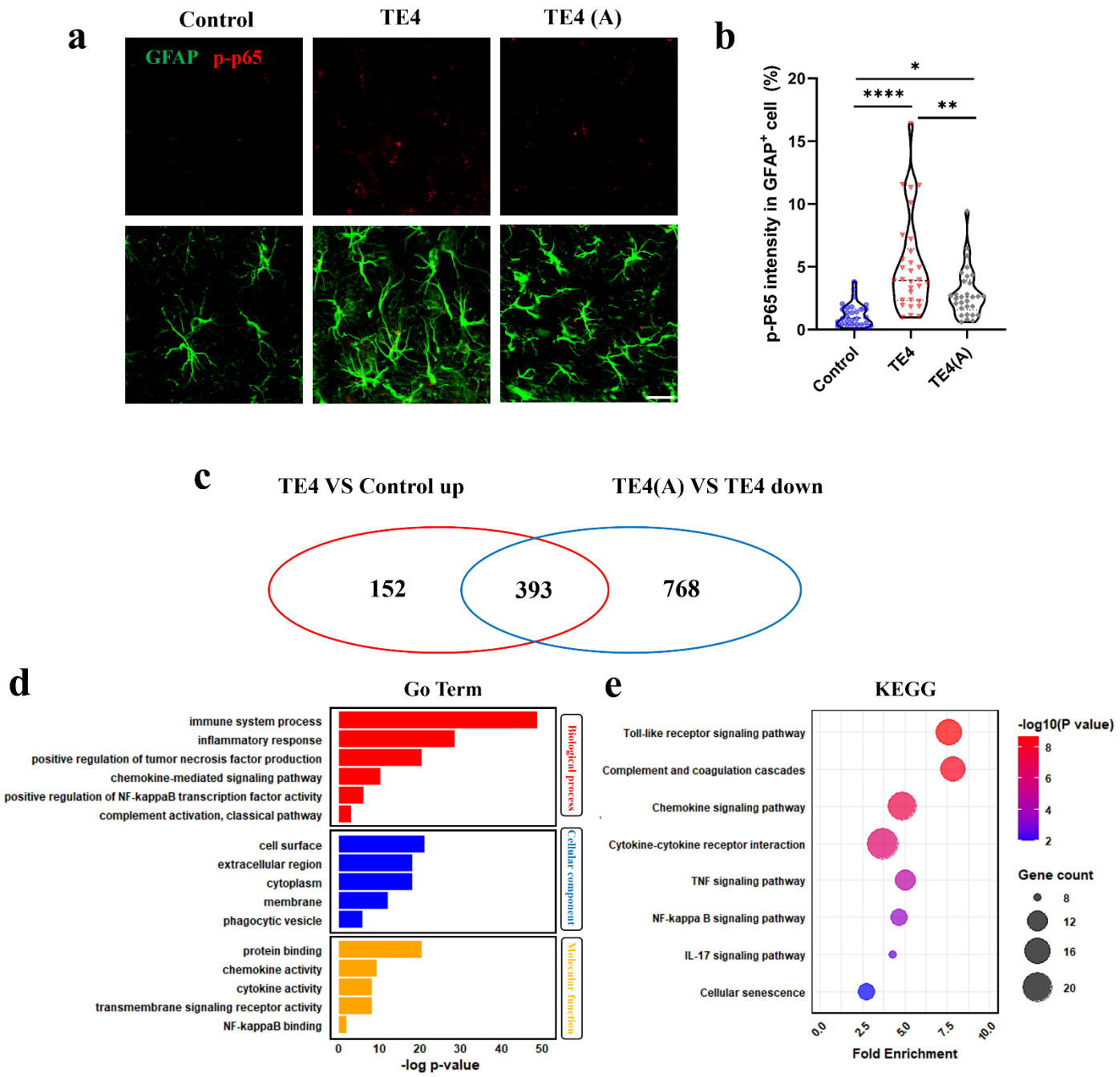

Supplementary Fig. 5 Anserine inhibited the activation of NF-κB pathway and complement system in astrocytes in TE4 mice.

a Representative images of GFAP and p-p65 co-staining in hippocampus area of 3 groups of mice (scale bar: 25 μm). **b** Quantification of p-p65 intensity in GFAP positive cells in each group, (n=30).**c** Numbers of common DEGs that were up-regulated in TE4 mice compared with control mice and down-regulated in TE4 (A) mice compared with TE4 mice. **d** and **e** Results of KEGG (**d**) and Go term analysis (**e**) using common DEGs. Data represent means ± SEM and were analyzed by one-way ANOVA with Tukey's multiple comparisons test. *p<0.05, **p < 0.01, ****p < 0.0001.

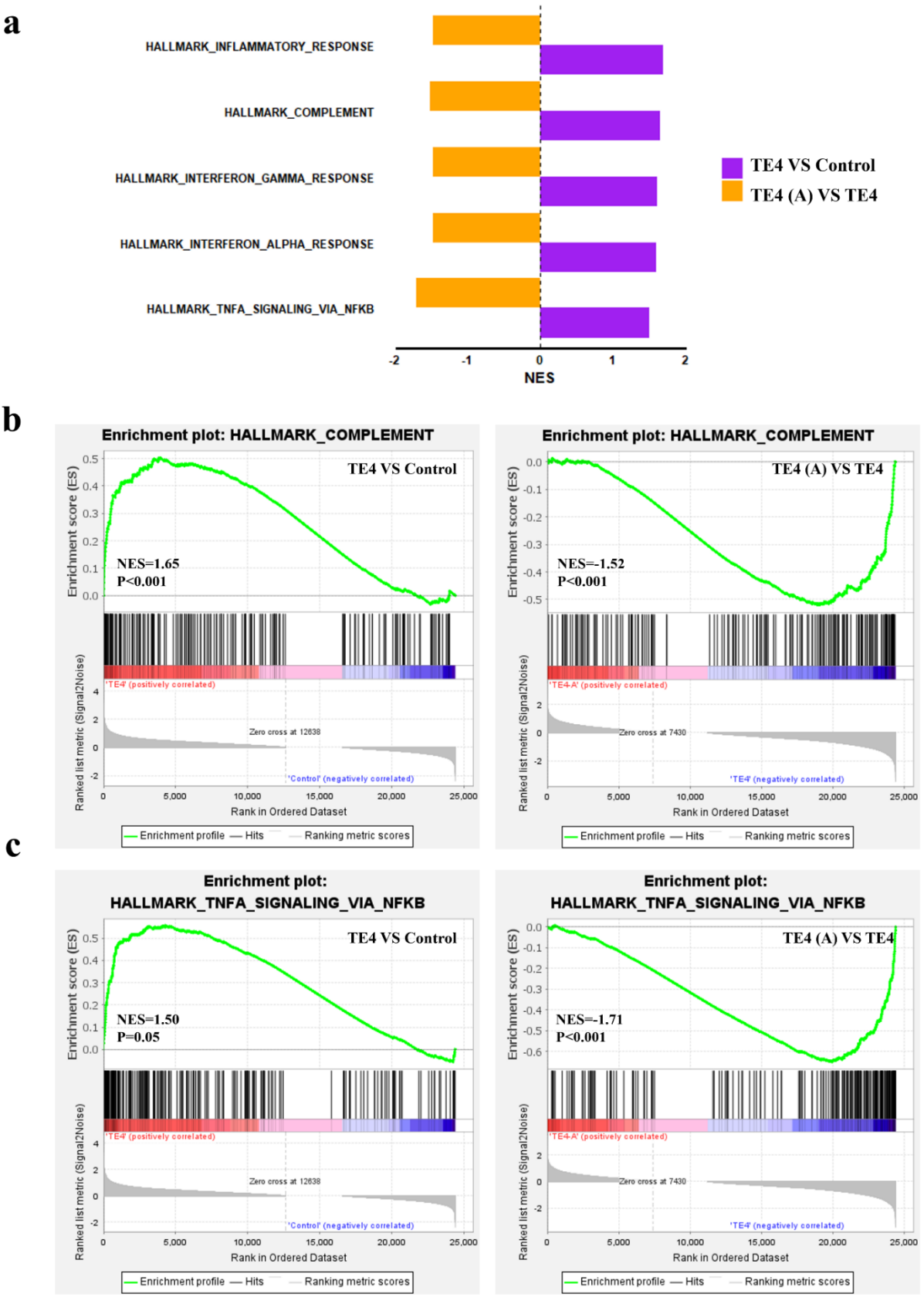

Supplementary Fig. 6 GESA results of isolated ASCA-2^{+} astrocytes.
a GESA results using the Hallmark database. The top 5 up-regulated gene sets were selected. **b** The result of GESA using the Hallmark database, focused on the complement system, the left showed the result of TE4 group VS Control group and the right showed the result of TE4 (A) group VS TE4 group. **c** The result of GESA using Hallmark database, focused on the NF-κB pathway, the left showed the result of TE4 group VS Control group and the right showed the result of TE4 (A) group VS TE4 group.

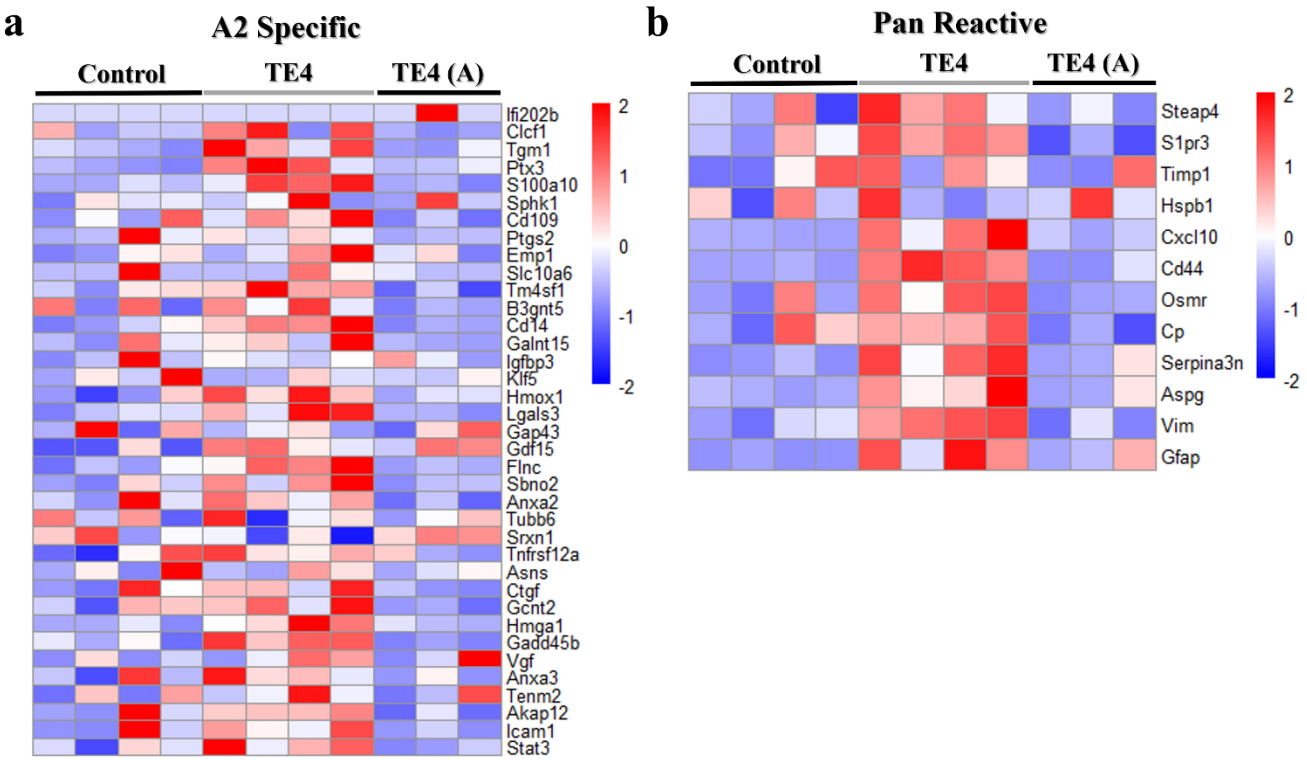

Supplementary Fig. 7 Additional results of RNA-Seq focused on astrocytes reactive markers.
a and **b** Heatmaps that show expression levels of selected A2 specific (**a**) and Pan reactive (**b**) markers in control, TE4 and TE4 (A) mice.

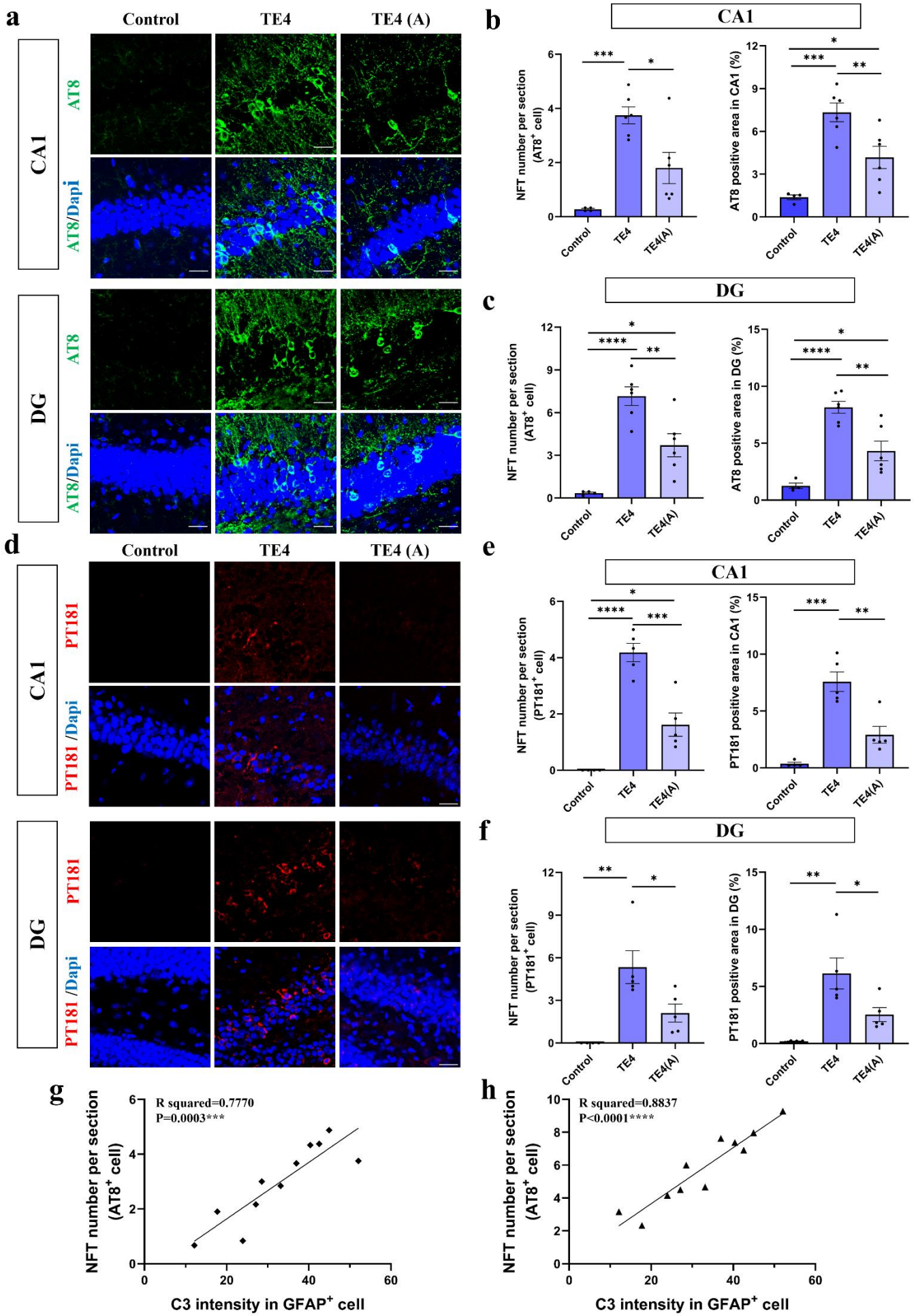
a
Control
TE4
TE4 (A)
CA1
AT8
AT8/Dapi
DG
AT8
AT8/Dapi
b
CA1
NFT number per section (AT8+ cell)
AT8 positive area in CA1 (%)
Control
TE4
TE4(A)
c
DG
NFT number per section (AT8+ cell)
AT8 positive area in DG (%)
d
Control
TE4
TE4 (A)
CA1
PT181
PT181 /Dapi
DG
PT181
PT181 /Dapi
e
CA1
NFT number per section (PT181+ cell)
PT181 positive area in CA1 (%)
f
DG
NFT number per section (PT181+ cell)
PT181 positive area in DG (%)
g
R squared=0.7770
P=0.0003***
NFT number per section (AT8+ cell)
C3 intensity in GFAP+ cell
h
R squared=0.8837
P<0.0001****
NFT number per section (AT8+ cell)
C3 intensity in GFAP+ cell

Supplementary Fig. 8 Attenuated tau pathology by suppressing astrocytic C3 secretion in TE4 mice
a Representative images of AT8 staining in CA1 and DG area of 3 groups of mice (scale bar: 25 μm). **b** and **c** Quantification of NFT number and AT8 positive stain area in CA1 (**b**) and DG (**c**) area in each group, (n=4-6). **d** Representative images of PT181 staining in CA1 and DG area of 3 groups of mice (scale bar: 25 μm). **e** and **f** Quantification of NFT number and PT181 positive stain area in CA1 (**e**) and DG (**f**) area in each group, (n=4-5). **g** and **h** The simple linear regression curve of NFT number in CA1 (**g**) and DG (**h**) area and C3 intensity in GFAP-positive cells of TE4 mice, (n=11). Data represent means ± SEM and were analyzed by one-way ANOVA with Tukey's multiple comparisons test. *$p < 0.05$, **$p < 0.01$, ***$p < 0.001$, ****$p < 0.0001$.

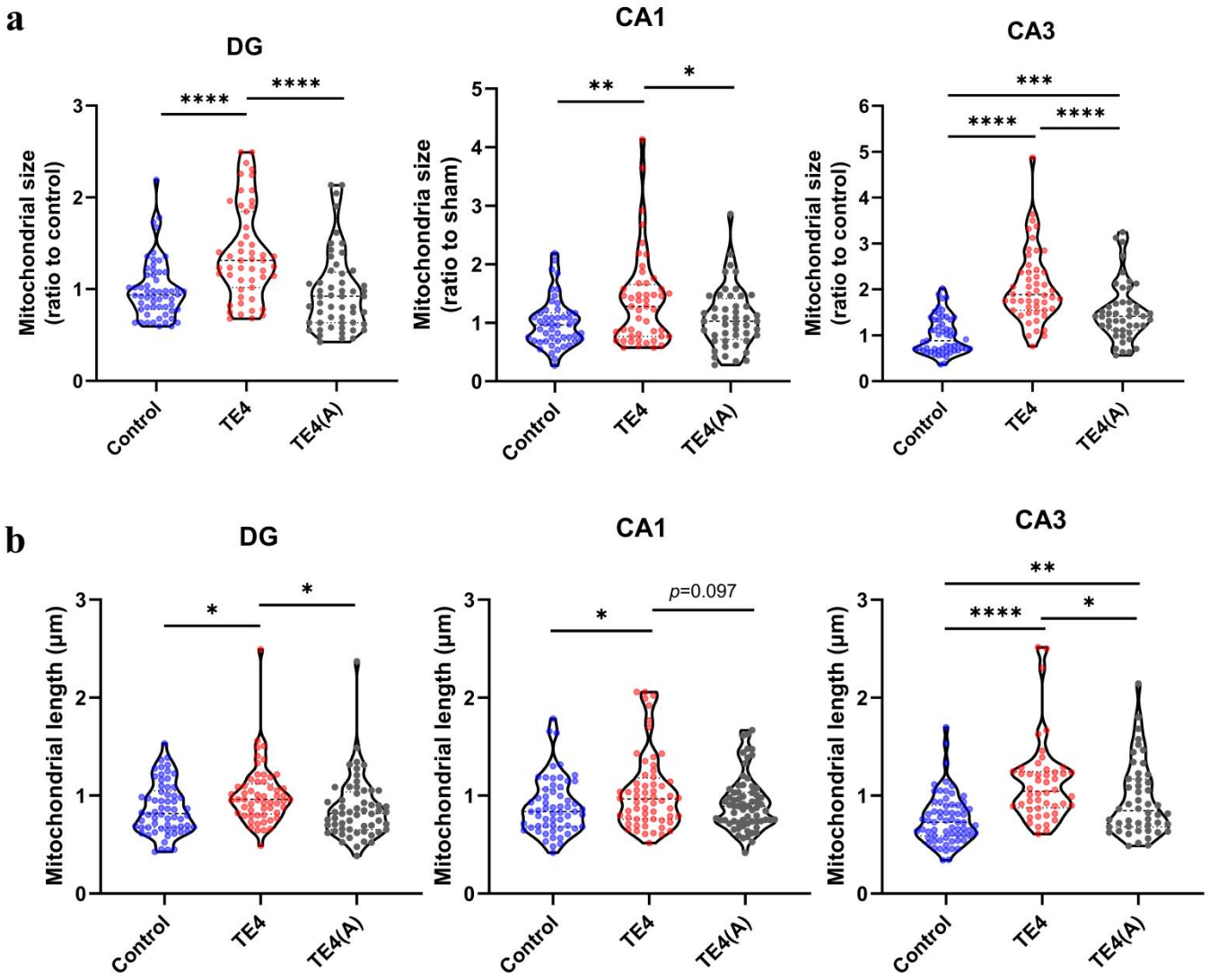

Supplementary Fig. 9 Downregulation of astrocytic C3 production prevented mitochondrial swelling in hippocampus neurons in TE4 mice.

a Quantification of mitochondrial size in DG, CA1 and CA3 area of 3 groups of mice, (n=46-60). **b** Quantification of mitochondrial length in DG, CA1 and CA3 area of 3 groups of mice, (n=48-67). Data represent means ± SEM and were analyzed by one-way ANOVA with Tukey's multiple comparisons test. *$p < 0.05$, **$p < 0.01$, ***$p < 0.001$, ****$p < 0.0001$.

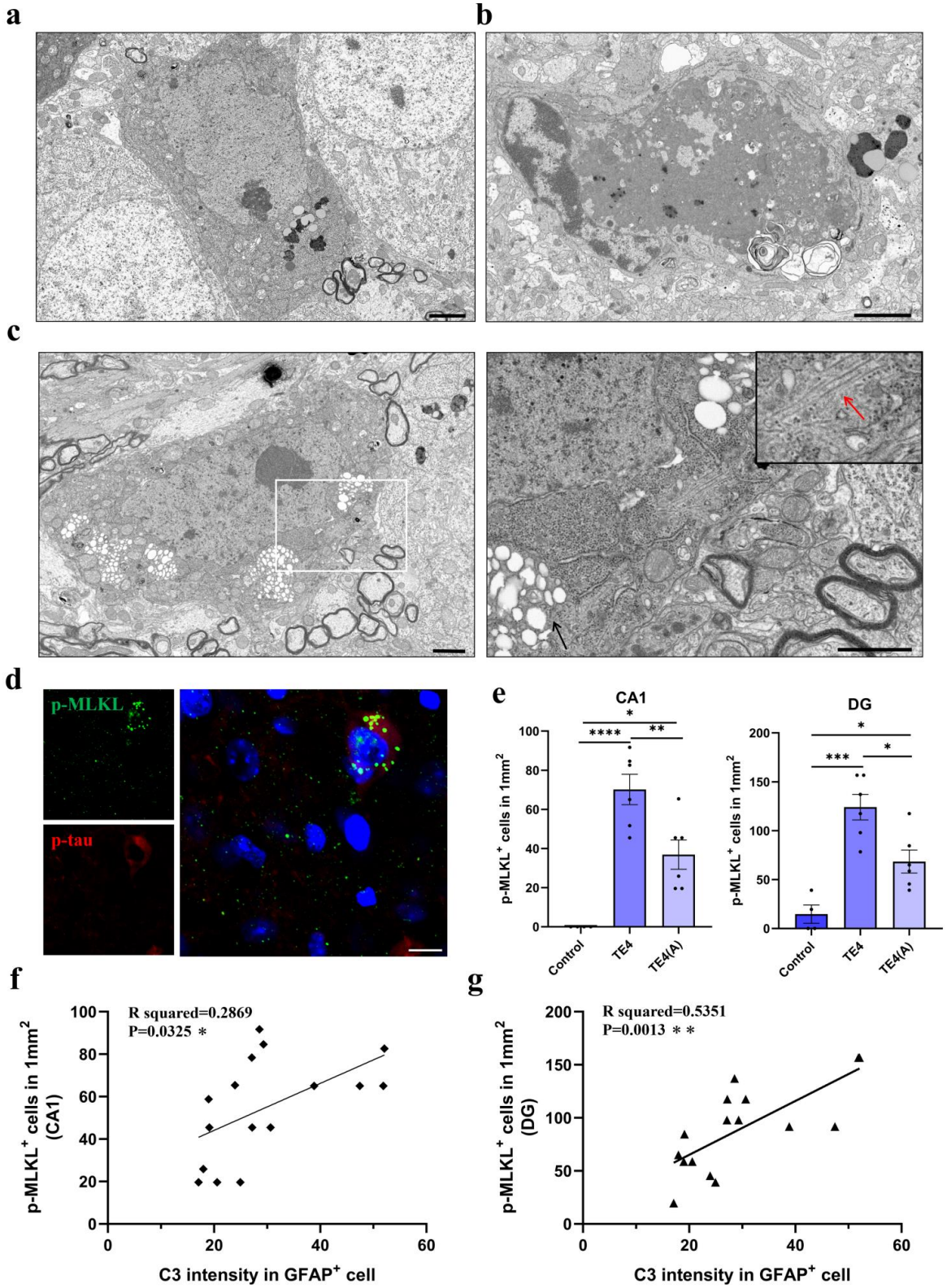

Supplementary Fig. 10 Suppression of astrocytic C3 production alleviated tau-mediated neuronal necroptosis in TE4 mice.

a and b Representative SEM image of hippocampal neurons of TE4 mice. **a** showed the neurodegeneration and **b** showed neuronal death (scale bar: 2 μm). **c** Representative electron microscopic images of hippocampal neurons in TE4 mice with necroptosis-like structure, (Scale bar: 1 μm). The red arrow showed tau fibers the and black arrow showed the cell vacuolization. **d** Representative images of P181T and p-MLKL co-staining in the hippocampus in TE4 mice (scale bar: 10 μm). **e** Quantification of p-MLKL positive-neurons in CA1 and DG area in each group, (n=4-6). **f** and **g** The simple linear regression curve of p-MLKL positive-neuron number in CA1 (**f**) and DG (**g**) area and C3 intensity in GFAP-positive cells of TE4 mice, (n=16). Data represent means ± SEM and were analyzed by one-way ANOVA with Tukey's multiple comparisons test. *$p < 0.05$, **$p < 0.01$, ***$p < 0.001$, ****$p < 0.0001$.

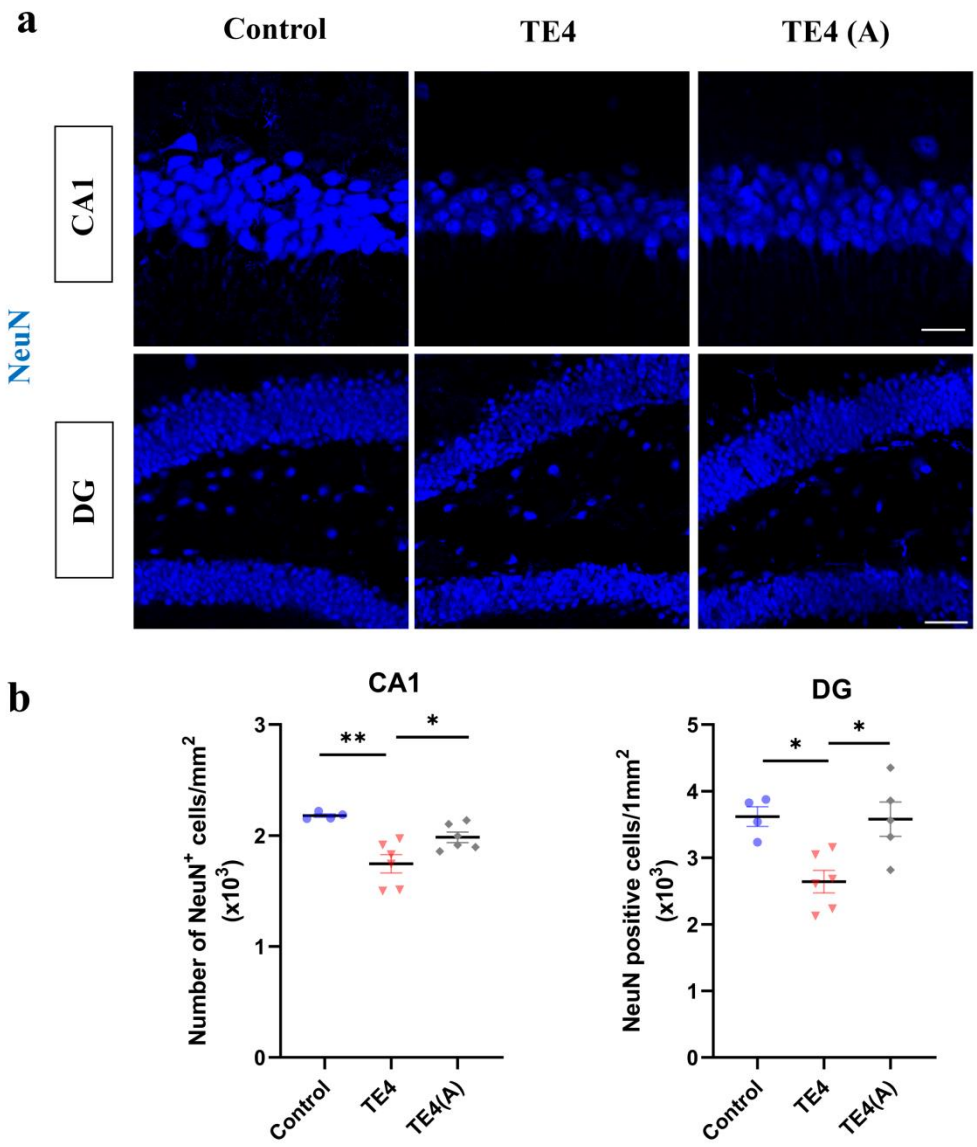

Supplementary Fig. 11 Anserine treatment increased neuronal density in TE4 mice

a Representative images of NeuN staining in CA1 and DG area of 3 groups of mice (scale bar: 25μm (up), 50μm (down)). **b** and **c** Quantification of neuron density in CA1 (**b**) and DG area (**c**) in each group, (n=4-6). Data represent means ± SEM and were analyzed by one-way ANOVA with Tukey's multiple comparisons test. *$p < 0.05$, **$p < 0.01$.

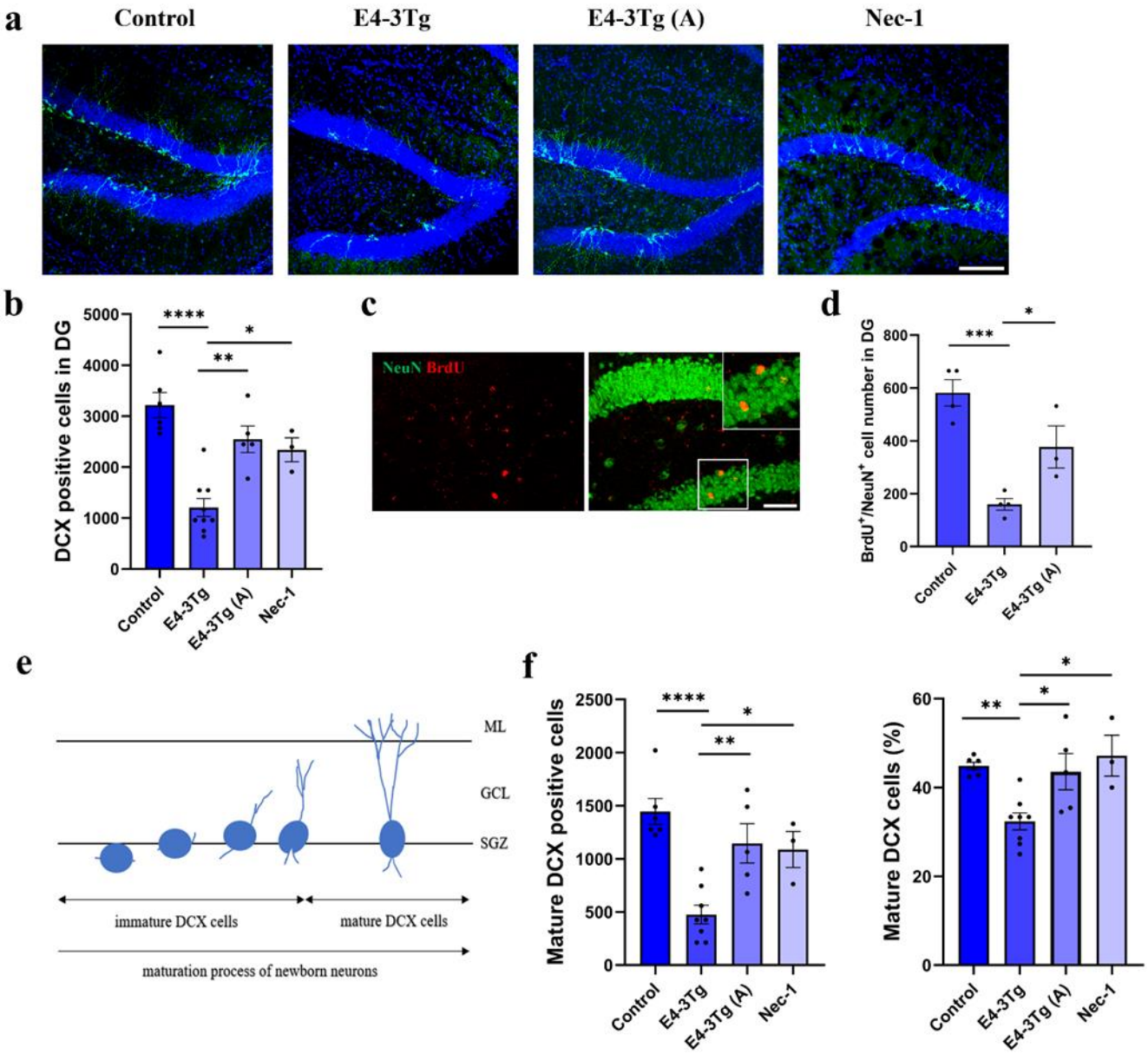

Supplementary Fig. 12 AHN impairment in E4-3Tg model mice.

a Representative image of DCX staining in DG area of control mice, E4-3Tg mice, E4-3Tg (A) mice and Nec-1 treated E4-3Tg mice (scale bar: 100 μm). **b** Quantification of DCX-positive cell number in DG in each group, (n=3-8). **c** Representative image of BrdU and NeuN co-staining in the DG area (scale bar: 50 μm). **d** Quantification of $BrdU^+/NeuN^+$ cell number in DG in each group, (n=3-4). **e** Definition of immature DCX cells and mature DCX cells. DCX-positive cells whose dendrites extend to the outer layer of the GCL and eventually extend into the ML were regarded as mature DCX cells. **f** Quantification of the number of mature DCX cells number (left) and mature DCX cells radio (right) in each group (n=3-8). Data represent means ± SEM and were analyzed by one-way ANOVA with Tukey's multiple comparisons test. *$p < 0.05$, **$p < 0.01$, ***$p<0.001$, ****$p < 0.0001$.

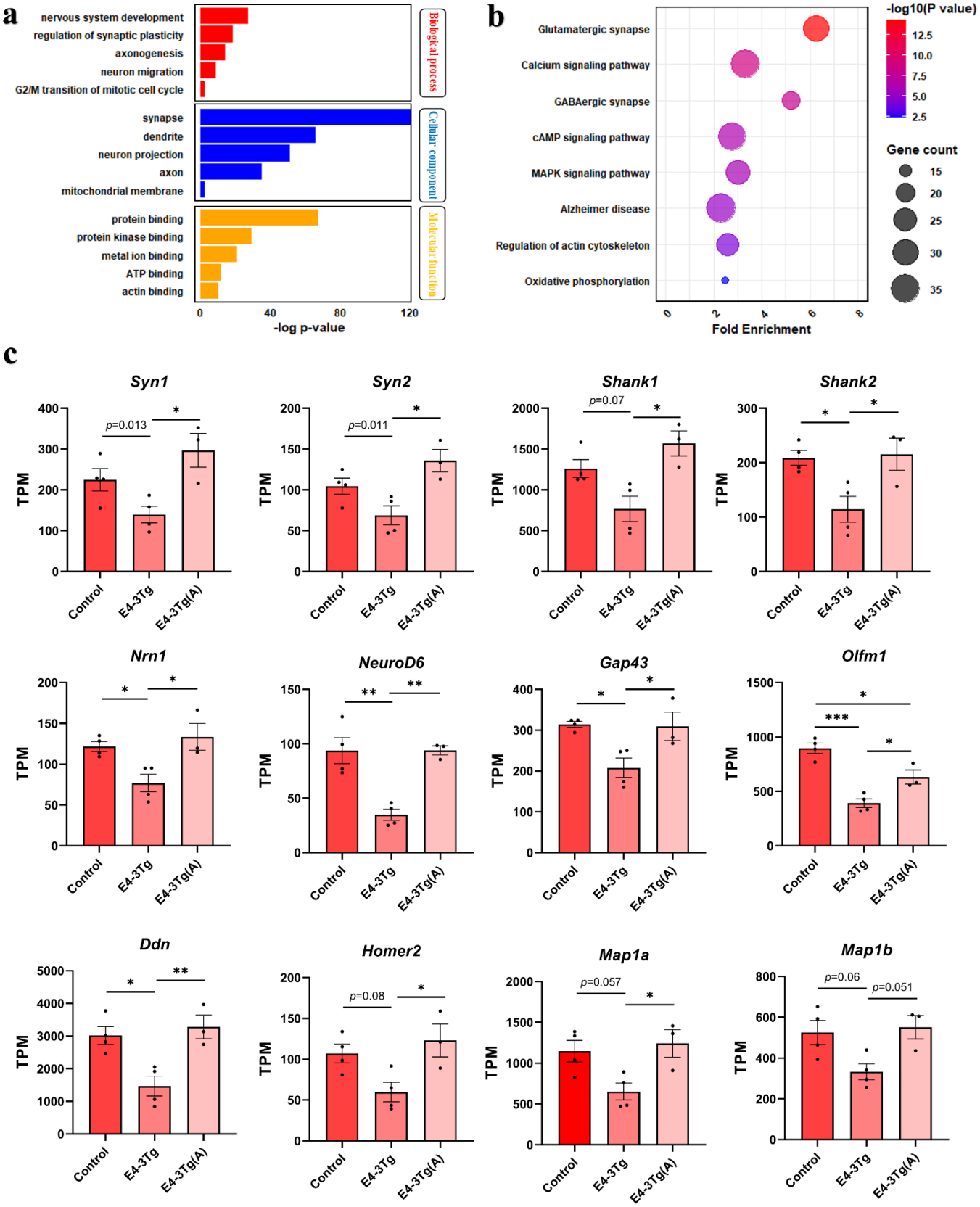

Supplementary Fig. 13 Dysfunction of Synaptogenesis in newborn neurons of E4-3Tg mice.
a-b Results of Go term (**a**) and KEGG analysis (**b**) using common DEGs that were down-regulated in E4-3Tg group compared with control group and up-regulated in E4-3Tg (A) mice compared with E4-3Tg mice. **c** Representative expression of genes related synaptogenesis and neuronal maturation in each group, (n=3-4). Data represent means ± SEM and were analyzed by one-way ANOVA with Tukey's multiple comparisons test. *$p < 0.05$, **$p < 0.01$, ***$p < 0.001$.

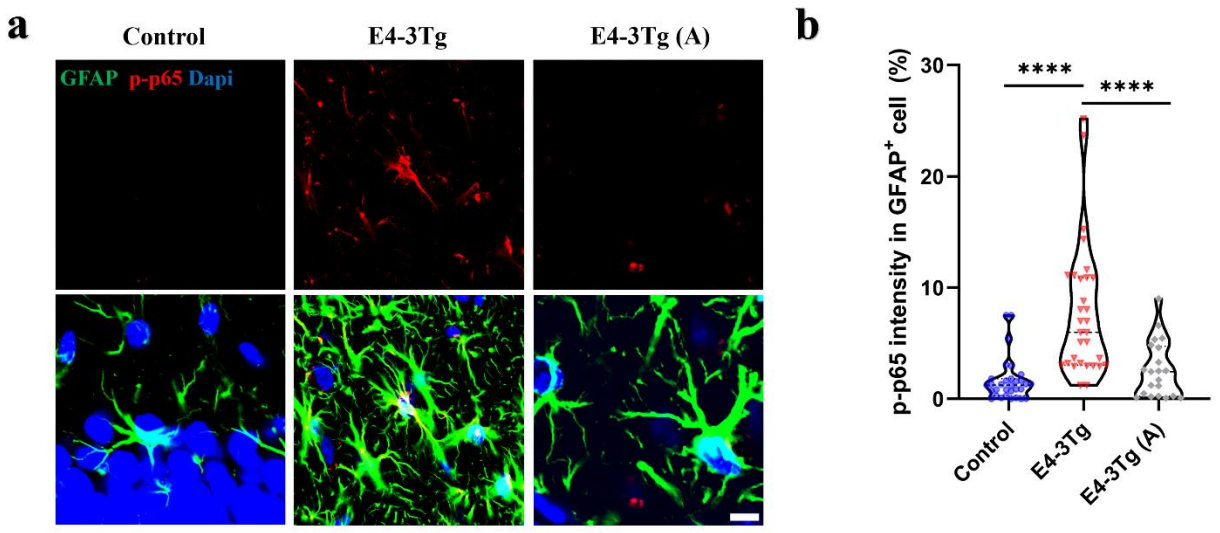

Supplementary Fig. 14 Anserine inhibited the activation of NF-κB pathway in astrocytes in E4-3Tg mice **a** Representative images of GFAP and p-p65 co-staining in DG area of 3 groups of mice (scale bar: 10 μm). **b** Quantification of p-p65 intensity in GFAP-positive cells in each group, (n=21-31). Data represent means ± SEM and were analyzed by one-way ANOVA with Tukey's multiple comparisons test. ****$p < 0.0001$.

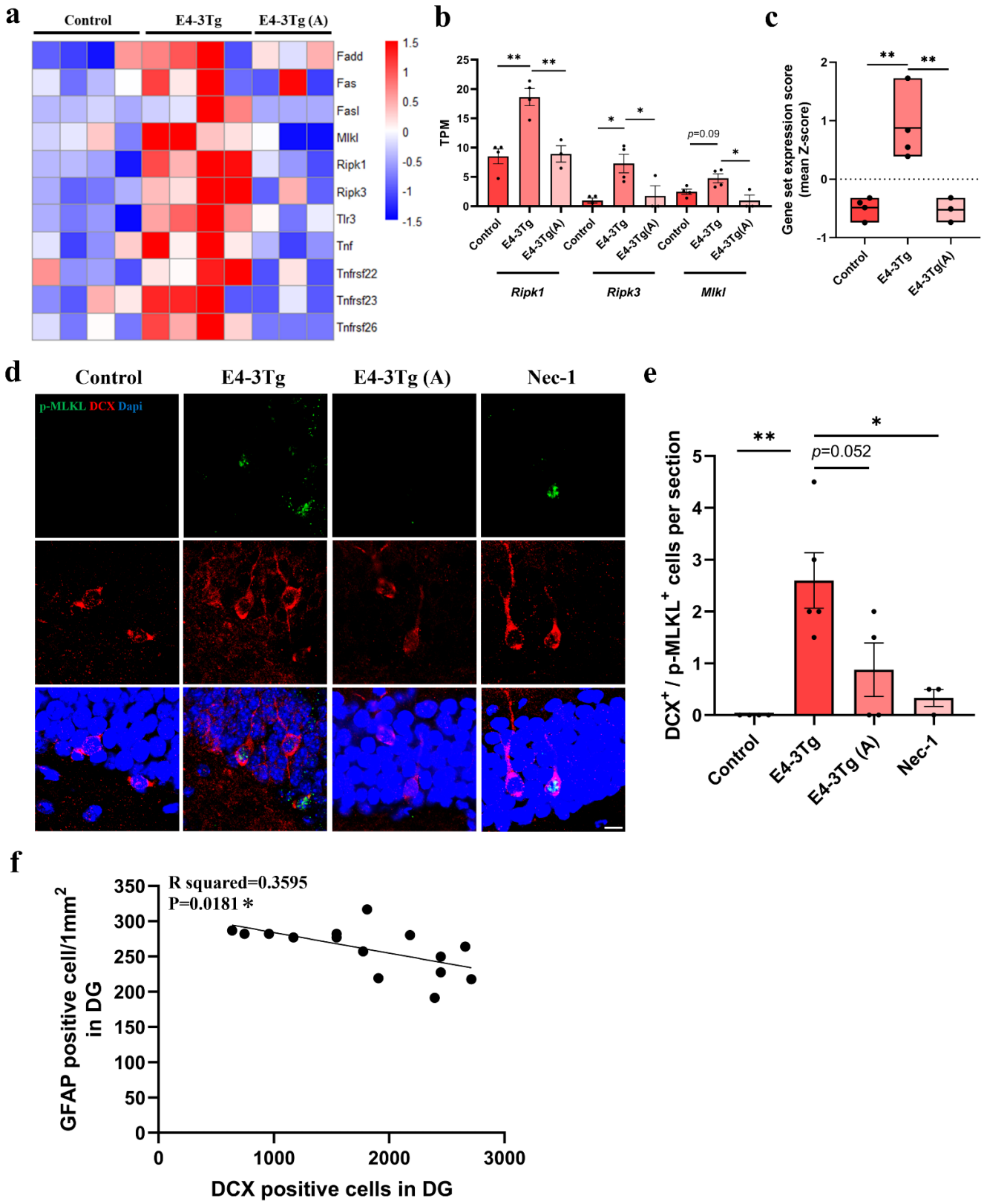

Supplementary Fig. 15 Anserine treatment prevented the activation of necroptosis pathway in new born neurons of E4-3Tg mice.

a Heatmap that shows expression levels of selected necroptosis markers control and E4-3Tg group. **b-c** TPM data (**b**) and gene set expression score (**c**) of necroptosis in control, E4-3Tg and E4-3Tg (A) group (n=3-4). **d** Representative image of DCX and p-MLKL co-staining in DG area of control mice, E4-3Tg mice, E4-3Tg (A) mice and Nec-1 treated E4-3Tg mice (scale bar: 10 μm). **e** Quantification of the number of DCX^+/ $p\text{-}MLKL^+$ cells in each group (n=3-5). **f** The simple linear regression curve of GFAP-positive cells number in DG area and DCX-positive cells number of E4-3Tg mice, (n=15). Data represent means ± SEM and were analyzed by one-way ANOVA with Tukey's multiple comparisons test. *$p < 0.05$, **$p < 0.01$.